The Astrophysical Journal, 823:72 (20pp), 2016 June 1 doi:10.3847/0004-637X/823/2/72

DYNAMICS AND TRANSIT VARIATIONS OF RESONANT EXOPLANETS

David Nesvorný[1] and David Vokrouhlický[2]
[1] Department of Space Studies, Southwest Research Institute, 1050 Walnut St., Ste 300, Boulder, CO 80302, USA; davidn@boulder.swri.edu
[2] Institute of Astronomy, Charles University, V Holešovičkách 2, CZ–18000 Prague 8, Czech Republic; vokrouhl@cesnet.cz
Received 2016 February 19; accepted 2016 March 31; published 2016 May 24

ABSTRACT

Transit timing variations (TTVs) are deviations of the measured midtransit times from the exact periodicity. One of the most interesting causes of TTVs is the gravitational interaction between planets. Here we consider a case of two planets in a mean motion resonance (orbital periods in a ratio of small integers). This case is important because the resonant interaction can amplify the TTV effect and allow planets to be detected more easily. We develop an analytic model of the resonant dynamics valid for small orbital eccentricities and use it to derive the principal TTV terms. We find that a resonant system should show TTV terms with two basic periods (and their harmonics). The resonant TTV period is proportional $(m/M_*)^{-2/3}$, where m and M_* are the planetary and stellar masses. For $m = 10^{-4} M_*$, for example, the TTV period exceeds the orbital period by about two orders of magnitude. The amplitude of the resonant TTV terms scales linearly with the libration amplitude. The ratio of the TTV amplitudes of two resonant planets is inversely proportional to the ratio of their masses. These and other relationships discussed in the main text can be used to aid the interpretation of TTV observations.

Key words: planets and satellites: detection – planets and satellites: dynamical evolution and stability

1. INTRODUCTION

Photometric observation of transits is one of the most powerful methods of planet detection. This method relies on a possibility that, if the planet's orbit is viewed nearly edge-on, the planet may repeatedly transit over the disk of its host star and periodically block a small fraction of the starlight. Thus, by monitoring the host star's brightness, the planet's presence can be revealed by a small dip in the photometric light curve. The main properties of the planet, such as its physical radius and orbital period, can be inferred from transit observations.

The spacing of transit light curves would be exactly the same over the course of observations if a planet moved on a strictly Keplerian orbit. Several dynamical effects, however, can produce deviations from the Keplerian case and induce transit timing variations (TTVs). TTVs were originally proposed as a nontransiting planet detection method (Miralda-Escudé 2002; Agol et al. 2005; Holman & Murray 2005), but they have found more use in validating the transiting planet candidates from NASA's *Kepler* mission (e.g., Holman et al. 2010; Lissauer et al. 2011). Only a handful of nontransiting planets so far have been detected and characterized from TTVs (e.g., Nesvorný et al. 2012, 2013).

Significant progress has been made in the theoretical understanding of the various dynamical causes of TTVs. These efforts were pioneered by Agol et al. (2005). Heyl & Gladman (2007) focused on a long-period interaction between planets and showed that the apsidal precession of their orbits can be detected only with a long TTV baseline. Nesvorný & Morbidelli (2008), on the other hand, developed a general analytic model for short-period TTVs and showed that they can be used, under ideal circumstances, to uniquely determine the mass and orbital parameters of the interacting planets.

Explicit analytic formulas for short-period TTVs are now available for zeroth- (Agol et al. 2005; Nesvorný & Vokrouhlický 2014; Deck & Agol 2015) and first-order terms (Agol & Deck 2016) in planetary eccentricities. The important case of near-resonant TTVs was highlighted in Lithwick et al. (2012) for the first-order resonances and in Deck & Agol (2016) and Hadden & Lithwick (2016) for the second-order resonances. The near-resonant TTV signal is a special case of the short-periodic variations when one harmonic becomes amplified because of a proximity of the system to a mean motion resonance. Vokrouhlický & Nesvorný (2014) considered a case of co-orbital planets and showed that co-orbital TTVs are expected to have a characteristic sawtooth profile (for horseshoe orbits).

While the analytic works cited above cover a wide range of dynamically plausible planetary configurations, none of them (except for Agol et al. 2005) considered the case of a fully resonant planetary system, where two (or more) orbits are inside a mean motion resonance (e.g., 2:1, 3:2). This case is important because planetary migration in a protoplanetary gas disk should bring early planets into resonances (e.g., Masset & Snellgrove 2001). Indeed, many known planetary systems are consistent with having resonant orbits (e.g., Winn & Fabrycky 2015). This motivates us to consider the resonant case. Our main goal is to understand how resonant TTVs arise and how their period and amplitude scale with planetary parameters.

The resonant case has not received much attention in the TTV literature so far, at least in part because the resonant interaction of planets is complex and not easily amenable to analytic calculations. The short-periodic or near-resonant TTV signals, for example, can be computed with the standard methods of perturbation theory, where the unperturbed (Keplerian) motion is inserted in the right-hand side of the dynamical equations, and a linear variation of the orbital elements is obtained by quadrature. This method fails for the fully resonant orbits mainly because the resonant dynamics is nonlinear.

Here, we take advantage of recent advances in the theoretical understanding of resonant dynamics (e.g., Batygin & Morbidelli 2013a; hereafter BM13) and derive approximate formulas for TTVs of a resonant pair of exoplanets. In Section 2, we first give a summary of resonant TTVs. The goal of this section is to highlight the main results of this work.

Sections 3 and 4 explain how we obtained these results. We first show how a fully analytic solution can be obtained for a first-order resonance (Section 3). We then proceed to expand the exact solution in the Fourier series and explicitly derive the periods and amplitudes of the leading TTV terms (Section 4). The application of these results to real planetary systems is left for future work.

2. SUMMARY OF RESONANT TTVS

Consider a planar system of two planets with masses m_1 and m_2 orbiting a central star with mass M_*. The two planets gravitationally interact to produce TTVs. The TTV signals of the two planets, δt_1 and δt_2, can be approximated by

$$\delta t_j = \frac{1}{n_j}(-\delta\lambda_j + 2\delta h_j) + \mathcal{O}(e_j), \quad (1)$$

where n_j is the mean orbital frequency of planet j, $h_j = e_j \sin\varpi_j$, λ_j is the mean longitude, e_j is the eccentricity, and ϖ_j is the longitude of periapsis. The observer is assumed to see the system edge-on and measures angles λ_j and ϖ_j relative to the line of sight. Expression (1) is valid for small orbital eccentricities and small variations of the orbital elements $\delta\lambda_j$ and δh_j (Nesvorný 2009).

Here we consider a case with two planets in a first-order mean motion resonance (such that $n_1/n_2 \simeq k/(k-1)$ with integer k) and proceed by calculating the variations of orbital elements that are due to the resonant interaction (Sections 3 and 4). The final expressions are given as the Fourier series with harmonics of two basic frequencies. As for $\delta\lambda_j$ we have

$$-\frac{1}{n_1}\delta\lambda_1 = \frac{3(k-1)}{\Lambda_1\nu}\frac{P_\tau}{2\pi}A_\Psi\left[(1+\epsilon)\sin ft - \frac{\epsilon}{4}\sin 2ft\right],$$
$$-\frac{1}{n_2}\delta\lambda_2 = -\frac{3k}{\Lambda_2\nu}\frac{P_\tau}{2\pi}A_\Psi\left[(1+\epsilon)\sin ft - \frac{\epsilon}{4}\sin 2ft\right]. \quad (2)$$

Here, $\nu = (3/2)[(k-1)^2 n_1/\Lambda_1 + k^2 n_2/\Lambda_2]$, $\Lambda_j = m_j\sqrt{GM_* a_j}$, a_j is the semimajor axis, G is the gravitational constant, P_τ is the period of resonant librations in scaled time units ($P_\tau \sim 2$–4 in most cases of interest; Section 3.7), A_Ψ is the amplitude of the resonant oscillations of action Ψ (ranging from zero for an exact resonance to >1, where the approximation used to derive Equation (2) starts to break down), f is the frequency of resonant librations, and $0 \leqslant \epsilon < 1$ encapsulates the emergence of higher-order harmonics of f.[3]

The resonant frequency f is given by

$$f = (\nu C^2)^{1/3}\frac{2\pi}{P_\tau}, \quad (3)$$

with

$$C = \frac{Gm_1m_2}{a_2}\sqrt{\frac{f_1^2}{\Lambda_1} + \frac{f_2^2}{\Lambda_2}}, \quad (4)$$

where f_1 and f_2 are the resonant coefficients of the Laplacian expansion of the perturbing function (Table 1). The scaling of the resonant period, $P = 2\pi/f$, with different planetary parameters is discussed in Section 3.7. For practical reasons, Equation (2) has been truncated at the first order in ϵ. Higher orders in ϵ and higher harmonics of the libration frequency can be computed using the methods described in Section 4.

Table 1
Coefficients f_1 and f_2 for Different Resonances

Res.	$\alpha_{\rm res}$	f_1	f_2
2:1	0.630	−1.190	0.428
3:2	0.763	−2.025	2.484
4:3	0.825	−2.840	3.283
5:4	0.862	−3.650	4.084
6:5	0.886	−4.456	4.885
7:6	0.902	−5.261	5.686

Note. In the second column, we report the semimajor axis ratio for an exact resonance. The coefficient values are given for $\alpha = a_1/a_2 = \alpha_{\rm res}$.

The second term in Equation (1) is related to the variation of eccentricities and apsidal longitudes of the two planets. In the most basic approximation (Section 4.3), it can be written as

$$\frac{2}{n_1}\delta h_1 = \frac{P_1\eta_1^{-\frac{1}{3}}}{\pi\sqrt{\Lambda_1}}\frac{AA_\Psi}{\sqrt{A^2+B^2}}C_{u,0}\sin(\theta_0 + f_\theta t),$$
$$\frac{2}{n_2}\delta h_2 = \frac{P_2\eta_1^{-\frac{1}{3}}}{\pi\sqrt{\Lambda_2}}\frac{BA_\Psi}{\sqrt{A^2+B^2}}C_{u,0}\sin(\theta_0 + f_\theta t), \quad (5)$$

where $P_j = 2\pi/n_j$ are the orbital periods, θ_0 is the initial value of $\theta = k\lambda_2 - (k-1)\lambda_1$, and f_θ is the frequency of θ defined in Equation (65). In the libration regime, $f_\theta \ll f$. The resonant TTVs can therefore be understood as a sum of the librational variations given in Equation (2) and a slower modulation of the TTV signal given in Equation (5). In Equation (5), $C_{u,0}$ is a coefficient of the order of unity (Equation (67) in Section 4.3). For small libration amplitudes, $A_\Psi C_{u,0} \simeq \sqrt{2\Psi_0}$, where Ψ_0 is the initial value of the resonant action Ψ defined in Equations (21) and (24). This means that, unlike in Equation (2), TTVs from the variation of eccentricities and apsidal longitudes do not vanish when $A_\Psi = 0$. The dependence of the TTV amplitude on planetary masses arises from A, B, and η_1 in Equation (5), where $A = f_1/\sqrt{\Lambda_1}$, $B = f_2/\sqrt{\Lambda_2}$, and $\eta_1 = \nu/C$.

Two main approximations were adopted to derive Equations (2) and (5). In the first approximation, we retained the lowest-order eccentricity terms in the resonant interaction of planets. In the second approximation, we assumed that the libration amplitudes are not very large and expanded the exact solution in the Fourier series. Both these approximations are tested in Section 5. Here we just illustrate the validity of the Fourier expansion for small libration amplitudes (Figures 1 and 2).

Let us briefly consider an application of our results to the TTV analysis. We assume that the photometric transits are detected for planets 1 and 2 and that the orbital periods inferred from the transit ephemeris are such that the orbital period ratio $P_2/P_1 \simeq k/(k-1)$ with small integer k (indicating near-resonant or resonant orbits). Furthermore, TTVs are assumed to be detected for both planets. To be specific, let us consider a

[3] Ideally, it would be useful to give the resonant TTV formulas in terms of the orbital elements, but these expressions are excessively complex. Here we therefore opt for expressing TTVs in terms of the orbital elements, A_Ψ and P_τ. The dependence on A_Ψ is linear, and P_τ admits only a narrow range of values in the libration zone.

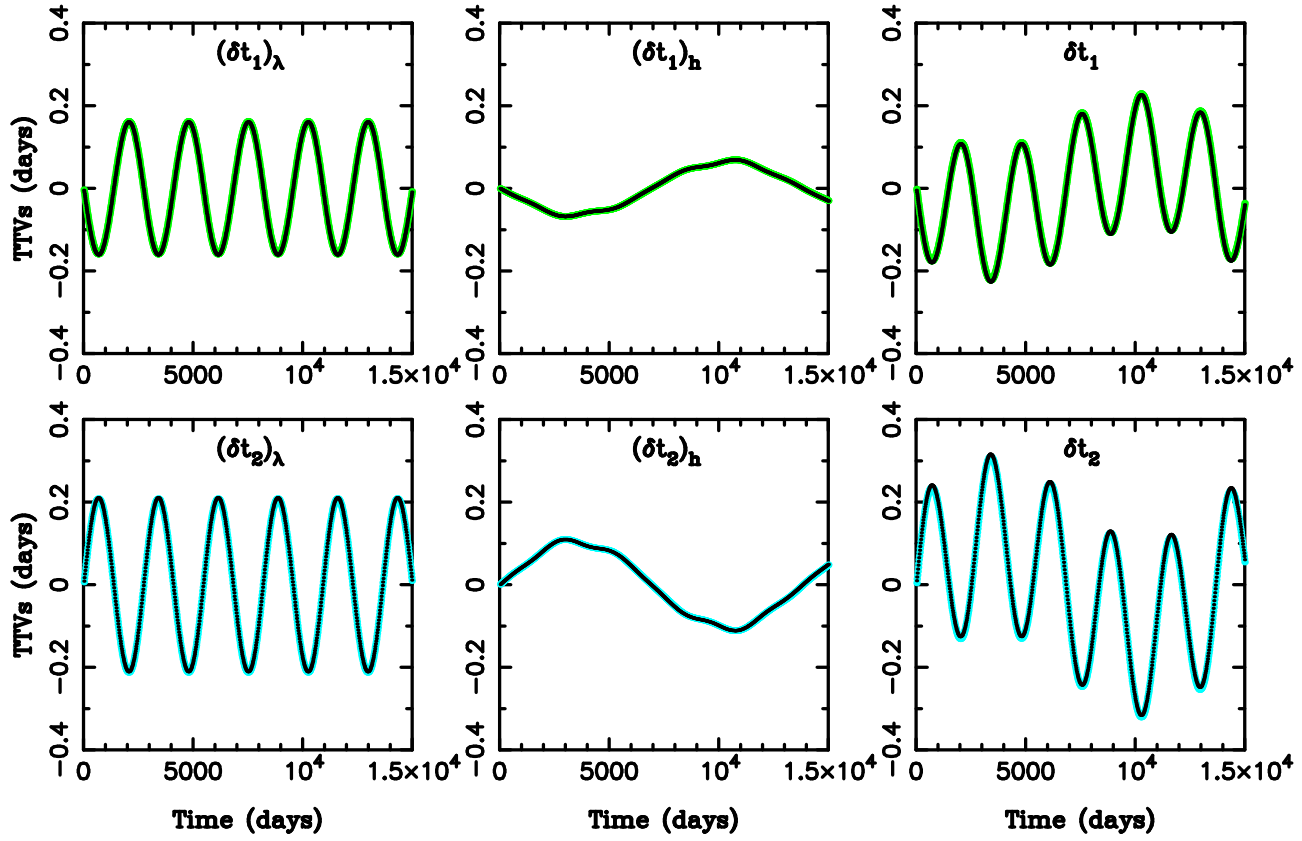

Figure 1. Demonstration of the validity of the analytic TTV formulas obtained in this work. Here we set $m_1 = m_2 = 10^{-5}\,M_*$ with $M_* = M_{\rm Sun}$. The initial orbital elements were $a_1 = 0.1$ au, $a_2 = 0.13115$ au, $e_1 = e_2 = 0.02$, $\lambda_1 = \pi$, $\lambda_2 = 0$, $\varpi_1 = 0$, and $\varpi_2 = \pi$. This orbital configuration corresponds to the libration regime in the 3:2 resonance ($k = 3$). The upper (lower) panel shows the results for the inner (outer) planet. The green and blue lines were computed by numerically integrating the differential equations corresponding to the resonant Hamiltonian (9) and (10). The black lines were obtained from the analytic TTV expressions (1) and (2) and a generalization of (5) derived in Section 4.3. From left to right, the panels show TTVs from $\delta\lambda_j$ and δh_j and their sum from Equation (1). The validity of the analytic model is excellent in this case because the resonant amplitude is relatively small ($A_\Psi \simeq 0.65$ with $\delta = 2.36$ and $\Psi_0 = 3.01$; see Section 3).

realistic case with the available TTV data spanning several years of observations, which is not long enough to resolve the frequencies related to the apsidal precession of orbits.

The first step of the TTV analysis is to apply the Fourier analysis to the TTV data. This may reveal that the TTV signal contains a basic period. In principle, this period can be one of the following two periods: (1) the superperiod defined as $P_{\rm s} = (k/P_2 - (k-1)/P_1)^{-1}$ (e.g., Lithwick et al. 2012) or (2) the resonant libration period $P = 2\pi/f$ with f defined in Equation (3). In the first case, the system is not in the libration regime of the resonance, and TTVs can therefore be interpreted using the expressions appropriate for the near-resonant dynamics (Lithwick et al. 2012; Agol & Deck 2016). The results described in this work apply in the second case. Section 3.7 explains how the libration period can be used to constrain planetary masses. Specifically, $P \propto (m/M_*)^{-2/3}$ (Agol et al. 2005; Holman et al. 2010), and therefore larger planetary masses imply shorter TTV periods. For the 2:1 resonance with $P_1 = 10$ days and $m_1 \simeq m_2 = 10^{-4}\,M_*$, for example, the libration period is $P \simeq 4.5$ years (Section 3.7).

In the next step, it can be useful to check if the Fourier analysis of the TTV data provides evidence for harmonics of the basic period. If that is the case, this can indicate that the libration amplitude is relatively large. A comparison of the amplitudes of different harmonics can then be used to constrain the parameter ϵ in Equation (2), which is related to the libration amplitude via the equations reported in Appendix A.

We then proceed by comparing the TTV amplitudes of the two planets. From Equation (2) we have that $\delta\lambda_1/\delta\lambda_2 \simeq -[(k-1)/k]^{2/3} m_2/m_1$. The TTV amplitude ratio therefore constrains the ratio of planetary masses (Agol et al. 2005). Figure 3 shows how the TTV amplitudes depend on planetary masses. For $m_1 \ll m_2$, we obtain from Equation (2) that the TTV amplitudes of the inner and outer planets, A_1 and A_2, are

$$A_1 = \frac{P_1}{2\pi}\frac{P_\tau}{\pi}\frac{A_\Psi}{k-1},$$
$$A_2 = \frac{P_2}{2\pi}\frac{P_\tau}{\pi}\frac{\sqrt{\alpha}A_\Psi}{k-1}\frac{m_1}{m_2}, \qquad (6)$$

where we denoted $\alpha = a_1/a_2$. This means that the TTV amplitude of the inner planet is independent of the masses, while that of the outer planet constrains m_1/m_2. For $P_1 = 10$ days, $P_\tau = 3$, and $A_\Psi = 1$, $A_1 = 1.52/(k-1)$ days for a k:$(k-1)$ resonance. A similar analysis can be performed for $m_1 \gg m_2$.

In addition to the dependence on masses, the TTV amplitudes (linearly) depend on the libration amplitude A_Ψ. We therefore expect that some degeneracy should exist between the planetary mass and libration amplitude, with large TTV amplitudes being produced either by large masses or large libration amplitudes. This degeneracy can be broken if the libration frequency harmonics are detected, providing

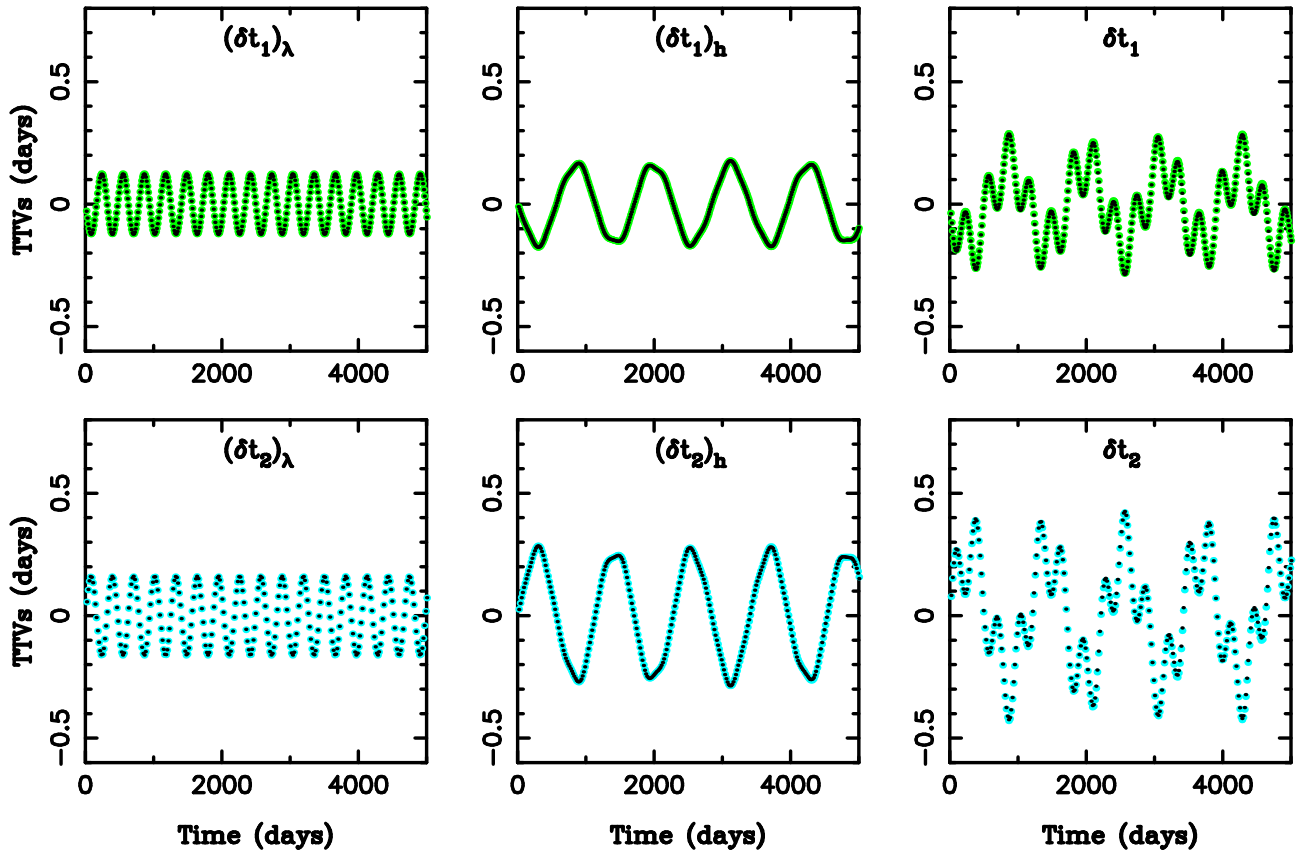

Figure 2. Same as Figure 1 but with $m_1 = m_2 = 3 \times 10^{-4}\, M_*$, $M_* = M_{\rm Sun}$, $a_1 = 0.1$ au, $a_2 = 0.132$ au, $e_1 = e_2 = 0.05$, $\lambda_1 = \pi$, $\lambda_2 = 0$, $\varpi_1 = 0$, and $\varpi_2 = \pi$. This corresponds to $A_\Psi \simeq -0.65$, $\delta \simeq 1.38$, and $\Psi_0 \simeq 1.96$ (Section 3). The periods are shorter in this plot than in Figure 1 because the two planets were given larger masses.

constraints on the libration amplitude, or if the measured TTV signal also contains short-period (chopping) terms (e.g., Nesvorný et al. 2013). A detailed analysis of this problem is left for future work.

3. ANALYTIC MODEL OF RESONANT DYNAMICS

Here we discuss a Hamiltonian model of the resonant dynamics. Our approach closely follows the work of BM13. We take several shortcuts to simplify the reduction of the Hamiltonian to an integrable system. Then, in Section 3.6, we present an exact analytic solution. This solution is used in Section 4 to derive Equations (2) and (5).

3.1. Hamiltonian Formulation of the Problem

The Poincaré canonical variables of two planets orbiting their host star are denoted by $(\boldsymbol{r}_0, \boldsymbol{r}_1, \boldsymbol{r}_2; \boldsymbol{p}_0, \boldsymbol{p}_1, \boldsymbol{p}_2)$. The coordinate vector $\boldsymbol{r}_0$ defines the host star's position with respect to the system's barycenter. Vectors $\boldsymbol{r}_1$ and $\boldsymbol{r}_2$ are the position vectors of the two planets relative to their host star. The momentum $\boldsymbol{p}_0$ is the total linear momentum of the system ($\boldsymbol{p}_0 = 0$ in the barycentric inertial frame). Momenta $\boldsymbol{p}_1$ and $\boldsymbol{p}_2$ are the linear momenta of the two planets in the barycentric inertial frame. The Poincaré variables are canonical, which can be demonstrated by calculating their Poisson brackets.

Using the Poincaré variables, the differential equations governing the dynamics of the two planets can be conveniently written in a Hamiltonian form, where the total Hamiltonian is a sum of the Keplerian and perturbation parts, $\mathcal{H} = \mathcal{H}_{\rm K} + \mathcal{H}_{\rm per}$, with

$$\mathcal{H}_{\rm K} = \sum_{j=1}^{2} \left(\frac{p_j^2}{2\,\mu_j} - G\,\frac{\mu_j M_j}{r_j} \right), \tag{7}$$

and

$$\mathcal{H}_{\rm per} = \frac{\boldsymbol{p}_1 \cdot \boldsymbol{p}_2}{M_*} - G\,\frac{m_1 m_2}{|\boldsymbol{r}_1 - \boldsymbol{r}_2|}. \tag{8}$$

Here we denoted $M_j = m_j + M_*$ and the reduced masses $\mu_j = m_j M_*/M_j$, where $j = 1$ and 2 stand for the inner and outer planet, respectively.

We assume that the planets are near or in a first-order mean motion resonance such that the ratio of their orbital periods is $P_2/P_1 \simeq k/(k-1)$ for some integer $k \geqslant 2$. In terms of the osculating orbital elements, we have

$$\mathcal{H}_{\rm K} = -G\,\frac{\mu_1 M_1}{2a_1} - G\,\frac{\mu_2 M_2}{2a_2}, \tag{9}$$

where a_1 and a_2 are the semimajor axes of planets, and

$$\begin{aligned} \mathcal{H}_{\rm per} = & -G\,\frac{m_1 m_2}{a_2} \\ & \times \{ f_1\, e_1 \cos[k\lambda_2 - (k-1)\lambda_1 - \varpi_1] \\ & + f_2\, e_2 \cos[k\lambda_2 - (k-1)\lambda_1 - \varpi_2] \}, \end{aligned} \tag{10}$$

where e_1 and e_2 are the orbital eccentricities, λ_1 and λ_2 are the mean longitudes, and ϖ_1 and ϖ_2 are the longitudes of pericenter. In Equation (10) we only retained the two most

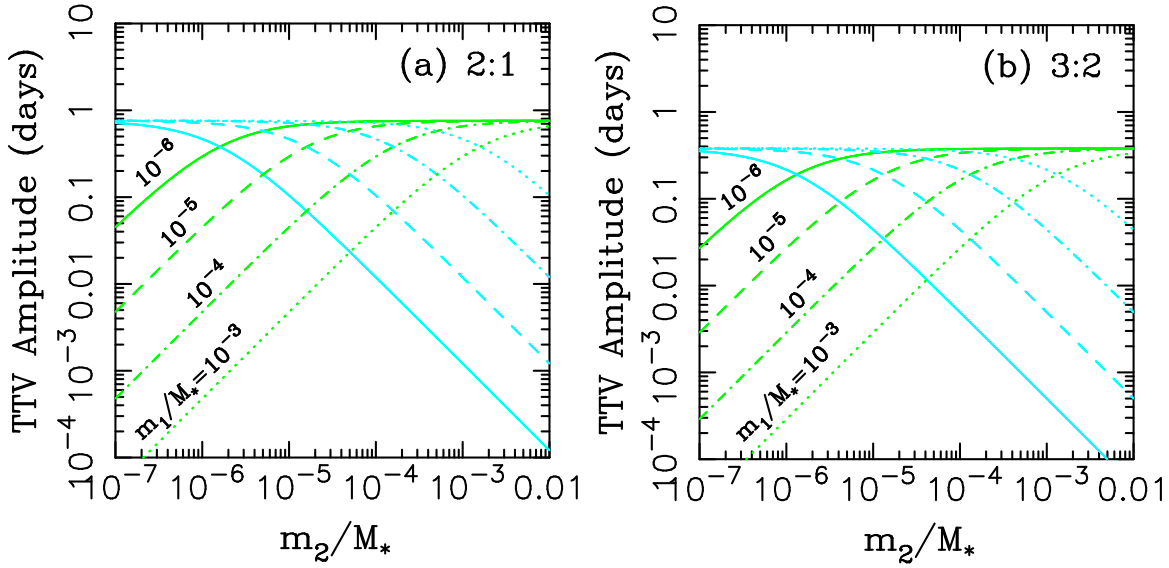

Figure 3. TTV amplitude from $\delta\lambda_j$ (Equation (2)) as a function of m_2/M_*. Here we assumed that $P_1 = 10$ days, $P_\tau = 3$, and $A_\Psi = 1$, and we computed the TTV amplitude for several different values of m_1/M_*: 10^{-6} (solid lines), 10^{-5} (dashed lines), 10^{-4} (dot-dashed lines), 10^{-3} (dotted lines). Panels (a) and (b) show the results for the 2:1 and 3:2 resonances, respectively. The green (blue) lines show the amplitude of δt_1 (δt_2).

important resonant terms and the lowest (first-order) eccentricity power. This expression is thus valid only near a specific resonance and for low orbital eccentricities of both planets. The planetary orbits are assumed to be in the same plane such that all inclination-dependent terms vanish.

The coefficients f_1 and f_2 are functions of the semimajor axis ratio $\alpha = a_1/a_2 < 1$ and can be written as

$$f_1 = -kb_{1/2}^{(k)}(\alpha) - \frac{\alpha}{2} D b_{1/2}^{(k)}(\alpha),$$
$$f_2 = \left(k - \frac{1}{2}\right) b_{1/2}^{(k-1)}(\alpha) + \frac{\alpha}{2} D b_{1/2}^{(k-1)}(\alpha) - \frac{\delta_{k,2}}{\alpha^{1/2}}, \quad (11)$$

where $b_{1/2}^{(k)}(\alpha)$ are the Laplace coefficients, $D = d/d\alpha$, and $\delta_{k,2}$ is the Kronecker symbol (e.g., Brouwer & Clemence 1961). The last term in the expression for f_2 only appears if $k = 2$ (2:1 resonance). The Laplace coefficients were computed using the recurrences described in Brouwer & Clemence (1961, Sections 15.7 and 15.8). Their values are reported in Table 1.

3.2. Resonant Variables

The resonant Hamiltonian discussed in the previous section needs to be written in canonical variables. The standard choice is the Delaunay elements

$$\Lambda_j = \mu_j \sqrt{GM_j a_j}, \quad \lambda_j,$$
$$\Gamma_j = \Lambda_j (1 - \sqrt{1 - e_j^2}), \quad \gamma_j = -\varpi_j. \quad (12)$$

Note that $\Gamma_j \simeq (1/2)\Lambda_j e_j^2$ for small e_j. The elements (Λ_j, Γ_j) are the canonical momenta, and (λ_j, γ_j) are the conjugated canonical coordinates.

The resonant Hamiltonian $\mathcal{H}$ written in terms of the Delaunay elements has four degrees of freedom (dof). Using canonical transformations, we will reduce it to an integrable one-dof system. We first perform a canonical transformation to the resonant canonical variables defined as

$$K_1 = \Lambda_1 + (k-1)(\Gamma_1 + \Gamma_2), \quad \lambda_1,$$
$$K_2 = \Lambda_2 - k(\Gamma_1 + \Gamma_2), \quad \lambda_2,$$
$$\Gamma_1, \quad \sigma_1 = k\lambda_2 - (k-1)\lambda_1 - \varpi_1,$$
$$\Gamma_2, \quad \sigma_2 = k\lambda_2 - (k-1)\lambda_1 - \varpi_2. \quad (13)$$

When the new variables are inserted in Equations (9) and (10), it becomes clear that the resonant Hamiltonian depends on σ_1 and σ_2, but not on λ_1 and λ_2. Therefore, $dK_j/dt = -\partial\mathcal{H}/\partial\lambda_j = 0$, and both momenta K_1 and K_2 are the new constants of motion. By summing them, we find that $K_1 + K_2 = \Lambda_1 + \Lambda_2 - \Gamma_1 - \Gamma_2$ is the total angular momentum of the system. Also, $kK_1 + (k-1)K_2 = k\Lambda_1 + (k-1)\Lambda_2 = \text{const.}$ implies that any small changes of the semimajor axes, δa_1 and δa_2, must be anticorrelated and have relative amplitudes such that $\delta a_1/\delta a_2 \simeq -\alpha_{\rm res}^{1/2}(k-1)m_2/km_1$, where we denoted $\alpha_{\rm res} = [(k-1)/k]^{2/3}$.

3.3. Approximation for Small Semimajor Axis Changes

The transformation to the resonant canonical variables produced a two-dof Hamiltonian $\mathcal{H} = \mathcal{H}(\sigma_1, \sigma_2; \Gamma_1, \Gamma_2)$. In the next step, we assume that any changes of the semimajor axes of planets are small. Specifically, we write $a_j = a_j^* + \delta a_j$, where a_j^* is some reference value and $\delta a_j \ll a_j^*$, insert this expression into the Keplerian part of the Hamiltonian (Equation (9)), and expand it in powers of δa_j. The first- and second-order terms in δa_j are retained. We then use $\delta a_j/a_j^* = 2\delta\Lambda_j/\Lambda_j^*$ and rewrite all expressions in terms of Λ_j^* and $\delta\Lambda_j$.[4] Finally, we substitute $\delta\Lambda_j \to \Lambda_j - \Lambda_j^*$ and drop all (dynamically unimportant) constant terms. This substitution is useful because it allows us to work with Λ_1 and Λ_2 instead of their variations $\delta\Lambda_1$ and $\delta\Lambda_2$. Finally, we express $\mathcal{H}_{\rm K}$ in terms of the canonical variables defined in Equation (13). This leads

[4] A general result can also be obtained by directly performing the Taylor expansion in $\Lambda_j = \Lambda_j^* + \delta\Lambda_j$.

to

$$\mathcal{H}_{\rm K} = n_0 + n_{\rm s}(\Gamma_1 + \Gamma_2) - \nu(\Gamma_1 + \Gamma_2)^2 \quad (14)$$

with

$$n_0 = 4(n_1K_1 + n_2K_2) - \frac{3}{2}\left[n_1\frac{K_1^2}{\Lambda_1^*} + n_2\frac{K_2^2}{\Lambda_2^*}\right],$$
$$n_{\rm s} = 4[kn_2 - (k-1)n_1] - 3\left[kK_2\frac{n_2}{\Lambda_2^*} - (k-1)K_1\frac{n_1}{\Lambda_1^*}\right],$$
$$\nu = \frac{3}{2}\left[(k-1)^2\frac{n_1}{\Lambda_1^*} + k^2\frac{n_2}{\Lambda_2^*}\right]. \quad (15)$$

Here we denoted $n_j = \sqrt{GM_j/a_j^{*3}}$ and $\Lambda_j^* = \mu_j\sqrt{GM_ja_j^*}$. The quantities n_j, $n_{\rm s}$, and ν are constant parameters. Note that $n_{\rm s}$ is related to the so-called *super* frequency, which is the expected frequency of the TTV signal for a pair of near-resonant planets (e.g., Lithwick et al. 2012). In addition to the usual term, $kn_2 - (k-1)n_1$, here $n_{\rm s}$ also includes a correction that is a second order in the eccentricity (through its dependence on K_1 and K_2).

As for $\mathcal{H}_{\rm per}$ in Equation (10), we have that $e_j = \sqrt{2\Gamma_j/\Lambda_j}$ for small eccentricity. In addition, because $\mathcal{H}_{\rm per}$ is already small, we do not need to retain terms proportional to δa_j (thus $\Lambda_j \to \Lambda_j^*$). The perturbation function then admits the following form:

$$\mathcal{H}_{\rm per} = -G\,\frac{m_1m_2}{a_2^*}[A\sqrt{2\Gamma_1}\cos\sigma_1 + B\sqrt{2\Gamma_2}\cos\sigma_2], \quad (16)$$

where we introduced constants $A = f_1/\sqrt{\Lambda_1^*}$ and $B = f_2/\sqrt{\Lambda_2^*}$.

3.4. Reducing Transformation

The Hamiltonian in Equations (14) and (16) has two degrees of freedom. It can be reduced to one dof by the following canonical transformations (Sessin & Ferraz-Mello 1984; Henrard et al. 1986; Wisdom 1986). First, we move from variables (σ_1, σ_2; Γ_1, Γ_2) to (y_1, y_2; x_1, x_2) such that

$$x_1 = \sqrt{2\Gamma_1}\cos\sigma_1, \quad y_1 = \sqrt{2\Gamma_1}\sin\sigma_1,$$
$$x_2 = \sqrt{2\Gamma_2}\cos\sigma_2, \quad y_2 = \sqrt{2\Gamma_2}\sin\sigma_2. \quad (17)$$

Second, we perform a reducing transformation to the new variables (v_1, v_2; u_1, u_2) defined as

$$u_1 = \frac{Ax_1 + Bx_2}{\sqrt{A^2+B^2}}, \quad v_1 = \frac{Ay_1 + By_2}{\sqrt{A^2+B^2}},$$
$$u_2 = \frac{Bx_1 - Ax_2}{\sqrt{A^2+B^2}}, \quad v_2 = \frac{By_1 - Ay_2}{\sqrt{A^2+B^2}}. \quad (18)$$

And last, we introduce new polar variables (ϕ_1, ϕ_2; Φ_1, Φ_2) such that

$$u_1 = \sqrt{2\Phi_1}\cos\phi_1, \quad v_1 = \sqrt{2\Phi_1}\sin\phi_1,$$
$$u_2 = \sqrt{2\Phi_2}\cos\phi_2, \quad v_2 = \sqrt{2\Phi_2}\sin\phi_2. \quad (19)$$

It can be shown that $\Gamma_1 + \Gamma_2 = \Phi_1 + \Phi_2$. Therefore, after dropping the first constant term in Equation (14) and rewriting Equation (16) in the new variables, the Hamiltonian becomes

$$\mathcal{H} = n_{\rm s}(\Phi_1 + \Phi_2) - \nu(\Phi_1 + \Phi_2)^2 - C\sqrt{2\Phi_1}\cos\phi_1, \quad (20)$$

where we denoted $C = Gm_1m_2\sqrt{A^2+B^2}/a_2^*$. Notably, the new Hamiltonian (20) is independent of ϕ_2, and the canonical momentum Φ_2 is therefore a new constant of motion. That is the magic of the reducing transformation.

The momenta Φ_1 and Φ_2 defined by the transformations discussed above can be expressed in a compact form:

$$\Phi_1 = \frac{1}{2}\frac{|Az_1 + Bz_2|^2}{A^2+B^2},$$
$$\Phi_2 = \frac{1}{2}\frac{|Bz_1 - Az_2|^2}{A^2+B^2}, \quad (21)$$

where $z_j = x_j + \imath y_j = \sqrt{2\Gamma_j}\exp\imath\sigma_j$. Condition $\Phi_2 = $ const. thus defines a circle in the plane of complex variables z_1 and z_2 and requires that $Bz_1 - Az_2$ lies on the circle at any time. Also, $\phi_1 = \arg(Az_1 + Bz_2)$ and $\phi_2 = \arg(Bz_1 - Az_2)$, where $\arg(z)$ denotes the argument of z.

3.5. Final Scaling

The Hamiltonian (20) depends on parameters $n_{\rm s}$, ν, and C. We rescale Φ_1 and time to bring the Hamiltonian to a simple form:

$$\mathcal{H} = -(\Psi - \delta)^2 - \sqrt{2\Psi}\cos\psi, \quad (22)$$

where the parametric dependence is expressed by a single parameter:

$$\delta = \eta_1^{2/3}\left[\frac{n_{\rm s}}{2\nu} - \Phi_2\right] \quad (23)$$

with $\eta_1 = \nu/C$. Here, $\psi = \phi_1$, and

$$\Psi = \eta_1^{2/3}\Phi_1. \quad (24)$$

The Hamiltonian equations are

$$\frac{d\psi}{d\tau} = \frac{\partial\mathcal{H}}{\partial\Psi} = -2(\Psi - \delta) - \frac{1}{\sqrt{2\Psi}}\cos\psi, \quad (25)$$
$$\frac{d\Psi}{d\tau} = -\frac{\partial\mathcal{H}}{\partial\psi} = -\sqrt{2\Psi}\sin\psi, \quad (26)$$

where τ relates to normal time t by

$$\tau = \eta_2^{1/3}t \quad (27)$$

with $\eta_2 = \nu C^2$. When a solution of Equations (25) and (26) is found, the scaling parameters η_1 and η_2 can be used to map the solution back to the original variables.

The Hamiltonian (22) and the corresponding Equations (25) and (26) have been extensively studied in the past. They are equivalent to the second fundamental model of resonance (Henrard & Lemaître 1983) and to the Andoyer model discussed in Ferraz-Mello (2007). Here we first consider the dynamical flow arising from this Hamiltonian and its dependence on δ. In the next section, we show that Equations (25) and (26) have an exact analytic solution in terms of the Weierstrass elliptic functions.

The equilibrium points of Equations (25) and (26) control the general structure of the dynamical flow. Since $d\Psi/d\tau = 0$ implies that $\sin\psi = 0$ in (26), the equilibrium points occur for

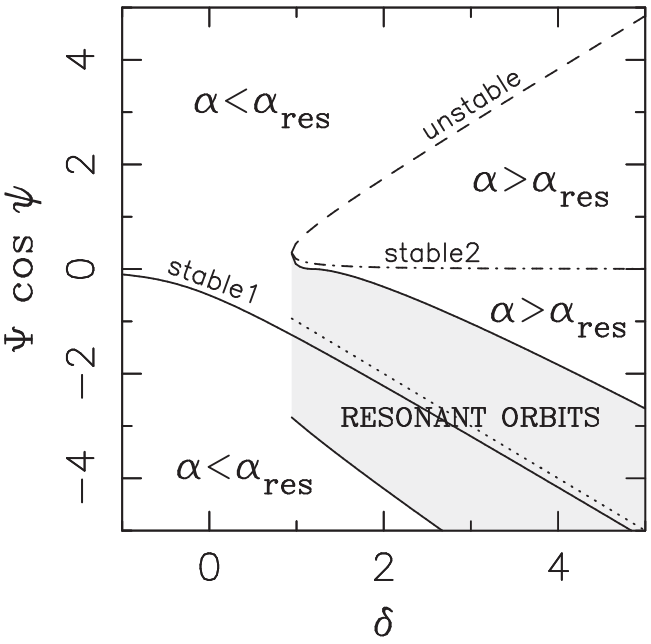

Figure 4. Equilibrium points and different dynamical regimes of the resonant Hamiltonian (22). The solid line denoted "stable 1" is the first stable equilibrium that exists for any value of δ. The second stable equilibrium, denoted by "stable 2," appears only for $\delta > \delta_* \simeq 0.945$. The dashed line is the unstable equilibrium. The gray area is the place where the resonant librations occur. The dynamical regime where the two orbits are just wide (narrow) of the resonance is labeled by $\alpha < \alpha_{\rm res}$ ($\alpha > \alpha_{\rm res}$). The dotted line is an approximation of the first equilibrium point, $\Psi_{\rm eq} = \delta$, that becomes progressively better with increasing δ.

$\psi = 0$ or π. The equilibrium values of Ψ are obtained from $d\psi/d\tau = 0$, which leads to a problem of finding the roots of a cubic equation $\Psi^3 - 2\delta\Psi^2 + \delta^2\Psi - 1/8 = 0$. There is only one (stable) equilibrium point for $\delta \leqslant \delta_* = (27/32)^{1/3} \simeq 0.945$. This equilibrium point is located at $\psi = \pi$ and $0 < \Psi < 1.26$ (Figure 4). The dynamical flow around the equilibrium point is simple. When projected to the $(\Psi\cos\psi, \Psi\sin\psi)$ plane,[5] the trajectories are concentric, slightly deformed circles centered on the equilibrium point (Figure 5(a)). Here, Ψ changes only slightly during each cycle, and ψ circulates in the clockwise direction for most initial conditions except for the ones located very close to the equilibrium point, where ψ oscillates around π.

For $\delta = \delta_*$, the stable equilibrium point is already substantially displaced from the origin. The dynamical transition is heralded by the appearance of a cusp trajectory (shown by a thin line in Figure 5(b)). Three equilibrium points appear for $\delta > \delta_*$, two of which are stable and one is unstable. The unstable equilibrium point is traversed by a separatrix (shown by thick lines in Figures 5(c) and (d)), which surrounds the truly resonant trajectories for which ψ librates around π. The stable equilibrium point in the center of the resonant island is a smooth extension of the equilibrium point from $\delta < \delta_*$ to $\delta > \delta_*$. It is located at $\psi = \pi$ and $\Psi = \Psi_{\rm eq}$, where $\Psi_{\rm eq}$ increases with δ (Figure 4). For large δ, $\Psi_{\rm eq} \simeq \delta$ (Henrard & Lemaître 1983).

[5] It is more common in this context to use $(\sqrt{2\Psi}\cos\psi, \sqrt{2\Psi}\sin\psi)$ because these variables are canonical.

3.6. Exact Analytic Solution

A rearrangement of Equations (25) and (26) shows that the momentum Ψ satisfies

$$\left(\frac{d\Psi}{d\tau}\right)^2 = f(\Psi), \tag{28}$$

with the right-hand side being a quartic polynomial:

$$f(\Psi) = a_0\Psi^4 + 4a_1\Psi^3 + 6a_2\Psi^2 + 4a_3\Psi + a_4. \tag{29}$$

The coefficients are

$$\begin{aligned} a_0 &= -1, \\ a_1 &= \delta, \\ a_2 &= -\frac{1}{3}[h_0 + 3\delta^2], \\ a_3 &= \frac{1}{2}[1 + 2\delta(h_0 + \delta^2)], \\ a_4 &= -[h_0 + \delta^2]^2, \end{aligned} \tag{30}$$

where $\mathcal{H}(\Psi_0, \psi_0) = h_0$ is the conserved energy, and (Ψ_0, ψ_0) is the initial condition. Equation (28) admits a general analytic solution (see Whittaker & Watson 1920, Section 20.4):

$$\Psi(\tau) = \Psi_0 + \frac{\mathcal{S}\sqrt{f_0}\,\wp'(\tau - \tau_0) + \frac{C_1}{2}\left[\wp(\tau - \tau_0) - \frac{C_2}{24}\right] + \frac{C_3}{24}f_0}{2\left[\wp(\tau - \tau_0) - \frac{C_2}{24}\right]^2 - \frac{C_4}{48}f_0}, \tag{31}$$

where $\Psi(\tau_0) = \Psi_0$, $f_0 = f(\Psi_0)$, $C_k = f^{(n)}(\Psi_0)$ is the nth derivative of f at $\Psi = \Psi_0$ ($n = 1, \ldots, 4$), and $\mathcal{S} = \mathrm{sgn}[\sin\psi_0]$ is the sign function (1 for $\sin\psi_0 > 0$ and -1 for $\sin\psi_0 < 0$). The time dependence of the solution is given in terms of the Weierstrass elliptic function $\wp(z)$ and $\wp'(z) = d\wp(z)/dz$, whose invariants are

$$\begin{aligned} g_2 &= a_0a_4 - 4a_1a_3 + 3a_2^2, \\ g_3 &= a_0a_2a_4 + 2a_1a_2a_3 - a_2^3 - a_0a_3^2 - a_1^2a_4. \end{aligned} \tag{32}$$

Interestingly, as far as we know, the general solution (31) has not been discussed in the literature. Ferraz-Mello (2007) mentioned a particular solution valid for $\sin\psi_0 = 0$, which implies that $f_0 = 0$ (see also Shinkin 1995).

The solution (31) is most conveniently evaluated using the relation of the Weierstrass functions to the Jacobi elliptic functions sn and cn. The form of the solution depends on the roots of the cubic equation $4z^3 - g_2z - g_3 = 0$, whose discriminant is $\Delta = g_2^3 - 27g_3^2$. There are three real roots $e_1 > e_2 > e_3$ for $\Delta > 0$. If $\Delta < 0$, there is one real root e_2 and a pair of complex roots $e_1 = \alpha + \imath\beta$ and $e_3 = \alpha - \imath\beta$ (Figure 6). In the first case ($\Delta > 0$), we have

$$\wp(\tau - \tau_0) = e_3 + \frac{e_1 - e_3}{\mathrm{sn}^2(u, k)}, \tag{33}$$

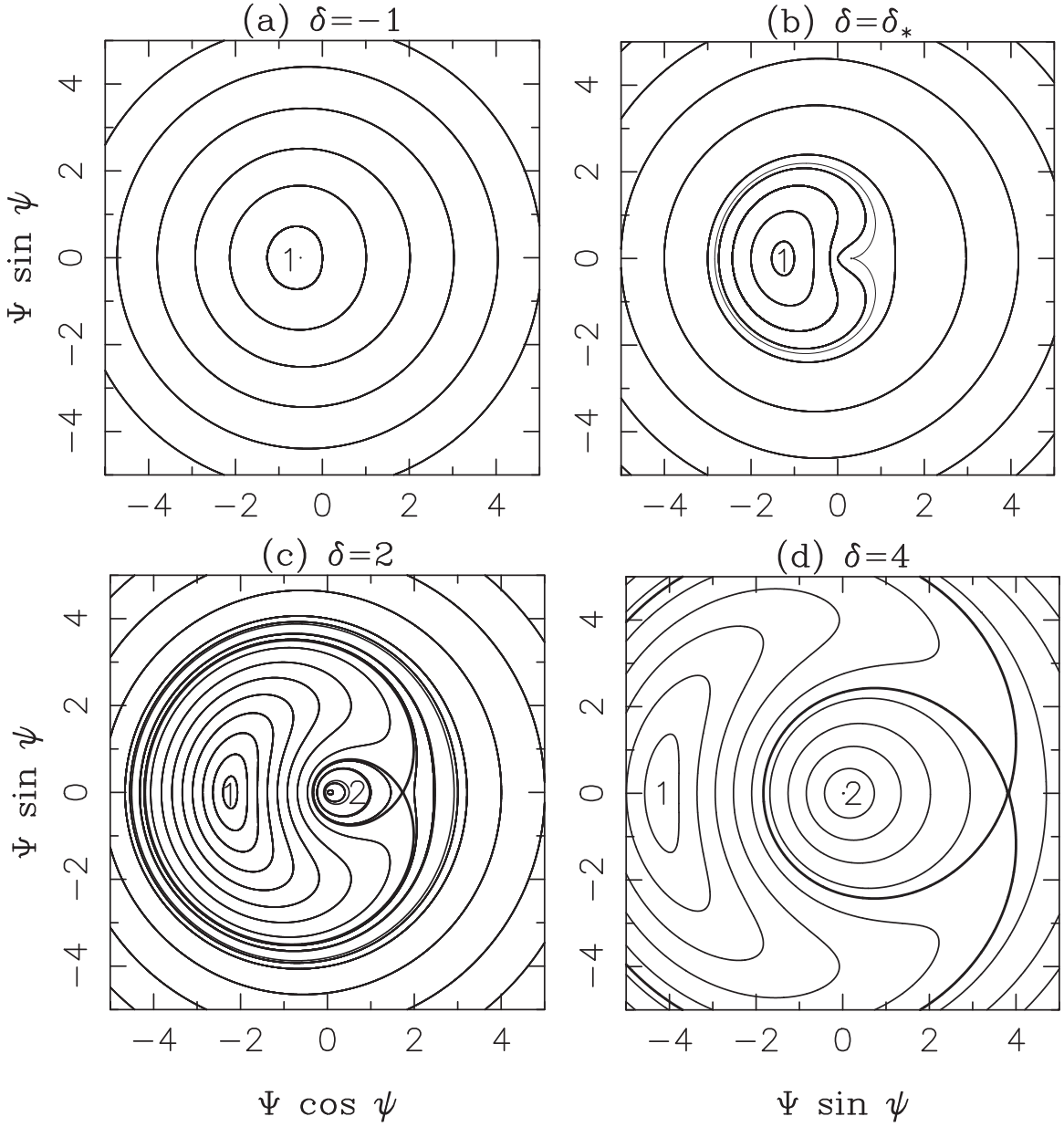

Figure 5. Dynamical portraits for four different values of parameter δ: (a) $\delta = -1$, (b) $\delta = \delta_*$, (c) $\delta = 2$, and (d) $\delta = 4$. The two stable equilibria are labeled "1" and "2." The cusp trajectory is shown by a thin line in panel (b). The separatrices are shown by bold lines in panels (c) and (d).

with $u = \sqrt{e_1 - e_3}\,(\tau - \tau_0)$ and modulus $k = \sqrt{\frac{e_2 - e_3}{e_1 - e_3}}$. In the second case ($\Delta < 0$), we have

$$\wp(\tau - \tau_0) = e_2 + \gamma\,\frac{1 + \mathrm{cn}(u, k)}{1 - \mathrm{cn}(u, k)}, \tag{34}$$

with $u = 2\sqrt{\gamma}\,(\tau - \tau_0)$, $\gamma = \sqrt{9\alpha^2 + \beta^2}$, and $k = \sqrt{\frac{1}{2} - \frac{3e_2}{4\gamma}}$. The Jacobi elliptic functions are computed following the numerical recipe from Press et al. (2007). The derivative $\wp'$ is obtained from the derivatives of the Jacobi functions.

3.7. Resonant Period

The solution (31) is periodic with a period

$$P_\tau = \frac{2\,\mathbb{K}(k)}{\sqrt{e_1 - e_3}}, \tag{35}$$

for $\Delta > 0$, and

$$P_\tau = \frac{2\,\mathbb{K}(k)}{\sqrt{\gamma}}, \tag{36}$$

for $\Delta < 0$. Here, $\mathbb{K}(k)$ is the complete elliptic integral of the first kind.

Figure 7 shows the period of small-amplitude librations around the stable equilibrium points. Away from the resonance and if the eccentricities are small, $n_s/(2\nu) \gg \Phi_2$, and the first bracketed term in Equation (23) outweighs the second. In this case, δ is related to the superfrequency and increases, in the absolute value, when the system moves away from the resonance. In this sense, δ is a measure of the distance from the resonance.[6]

[6] Inside the resonant island, n_s is small and δ is controlled by the contribution from Φ_2. Since $\Phi_2 \propto e^2$, δ is a measure of the orbital eccentricities inside the libration island.

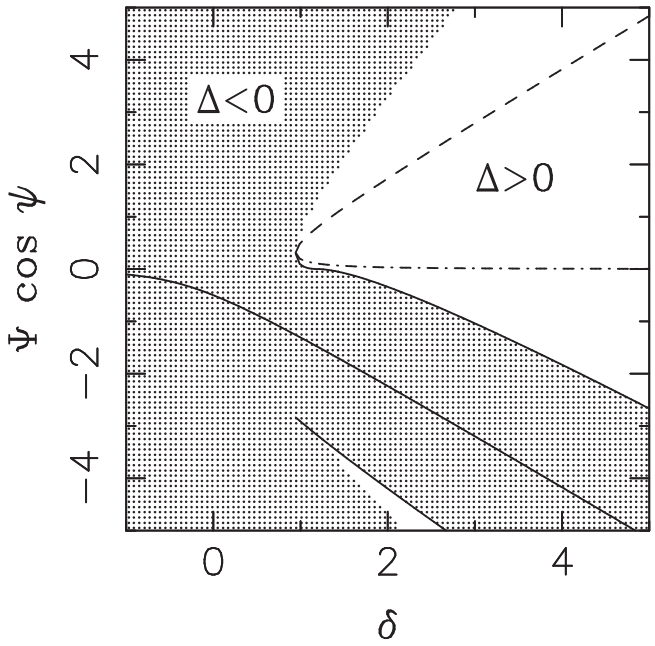

Figure 6. Range in parameters δ and $\Psi\cos\psi$ where Equation (31) admits different functional dependence on the Jacobi elliptic functions. In the void domain, the discriminant $\Delta > 0$, and Equation (33) applies. In the dotted domain, $\Delta < 0$, and Equation (34) applies. The lines show the location of the equilibrium points. See the caption of Figure 4 for more information.

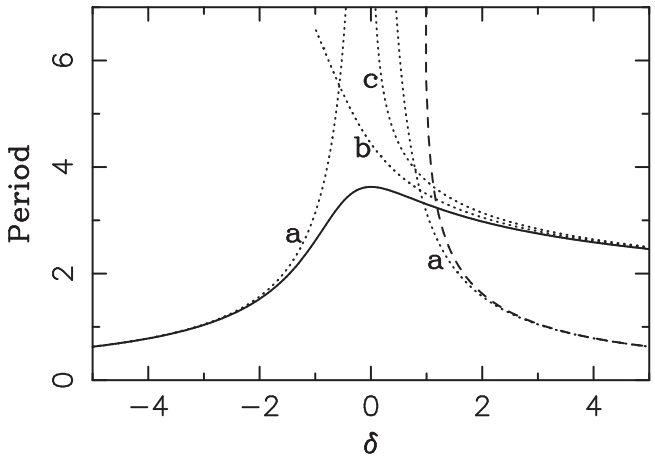

Figure 7. Period of small-amplitude librations around the stable equilibrium points. The solid and dashed lines show the periods in the libration ("stable 1" in Figure 4) and circulation domains ("stable 2" in Figure 4), respectively. The dotted lines are various approximations. The dotted line denoted by "a" is the superperiod approximation with $P_\tau = \pi/|\delta|$. The one denoted by "b" is an oscillator approximation $P_\tau = \pi\,(2/\Psi_{\rm eq})^{1/4}$, where $\Psi_{\rm eq}$ of the libration point is computed exactly for each δ. The dotted line "c" shows $P_\tau = \pi\,(2/\delta)^{1/4}$.

Negative values of δ imply that the planetary orbits are spaced more widely than the actual resonance ($P_2/P_1 > k/(k-1)$), while $\delta > 0$ means that the orbits are packed more tightly ($P_2/P_1 < k/(k-1)$). Also, $\delta \simeq \eta_2^{-1/3} n_s/2$ away from the resonance, and therefore the scaled period $P_\tau \simeq \pi/|\delta|$. This represents a very good approximation of the period if $\delta < -2$ or $\delta > 3$ (see Figure 7).

Inside the libration island for $\delta > \delta_*$, the period of small-amplitude librations decreases with δ (i.e., toward larger eccentricities). It can be approximated by $P_\tau = \pi(2/\Psi_{\rm eq})^{1/4}$, where $\Psi_{\rm eq}$ is the equilibrium value of Ψ (Figure 4). For large values of δ, $\Psi_{\rm eq} \simeq \delta$, and

$$P_\tau \simeq \pi\left(\frac{2}{\delta}\right)^{1/4}. \tag{37}$$

Figure 7 shows that this approximation works very well for $\delta > 3$.

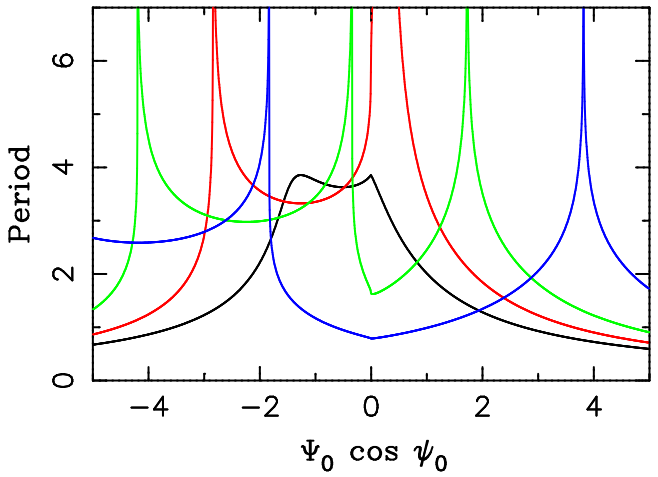

Figure 8. Period P_τ for different libration amplitudes. Here we set $\sin\psi_0 = 0$ and compute the period for different Ψ_0 from Equations (35) and (36). The different colors correspond to different δ values: $\delta = 0$ (black), $\delta = \delta_*$ (red), $\delta = 2$ (green), and $\delta = 4$ (blue). This figure can be compared to Figure 5, where the dynamical portraits are shown for the same values of δ.

The period P_τ for different libration amplitudes is plotted in Figure 8. The period is the shortest near the equilibrium point and increases with the libration amplitude. It becomes infinite on the separatrices. This corresponds to a situation when the amplitude of angle ψ becomes full π, and it takes infinitely long to reach the unstable equilibrium point at $\psi = 0$. Except for trajectories near the separatrix, the period values inside the libration island are $P_\tau \simeq 2.5$–4. They become shorter for $\delta > 5$ (i.e., for higher eccentricities).

When rescaled according to Equation (27), $P_t = \eta_2^{-1/3} P_\tau$ is the period of resonant librations in the normal time units (e.g., Julian days). It has the same dependence of P_τ on δ and amplitude that we discussed above and, in addition, contains an explicit dependence on the orbital period and planetary masses through the scaling parameter $\eta_2 = \nu C^2$. If $m_1 \ll m_2$, then

$$P_t \simeq P_1\,\frac{P_\tau}{2\pi}\left(\frac{m_2}{M_*}\right)^{-2/3}\left[\frac{3}{2}(k-1)^2 f_1^2\,\alpha^2\right]^{-1/3}. \tag{38}$$

If, on the other hand, $m_1 \gg m_2$, then

$$P_t \simeq P_2\,\frac{P_\tau}{2\pi}\left(\frac{m_1}{M_*}\right)^{-2/3}\left[\frac{3}{2}k^2 f_2^2\right]^{-1/3}. \tag{39}$$

The multiplication coefficients in the square brackets are $\simeq 1$ for $k = 2$ (2:1 resonance) and decrease with increasing k. This expresses a stronger interaction of orbits that are more tightly packed for larger values of k. According to Equations (38) and (39), the orbital periods P_1 and P_2 set the basic time unit for P_t.

The libration period scales with the mass of the more massive planet as $(m/M_*)^{-2/3}$ and is therefore shorter for a larger mass. It is insensitive to the mass of the lighter planet. If the masses of the two planets are comparable, then P_t will depend on their combination via the scaling parameter η_2.

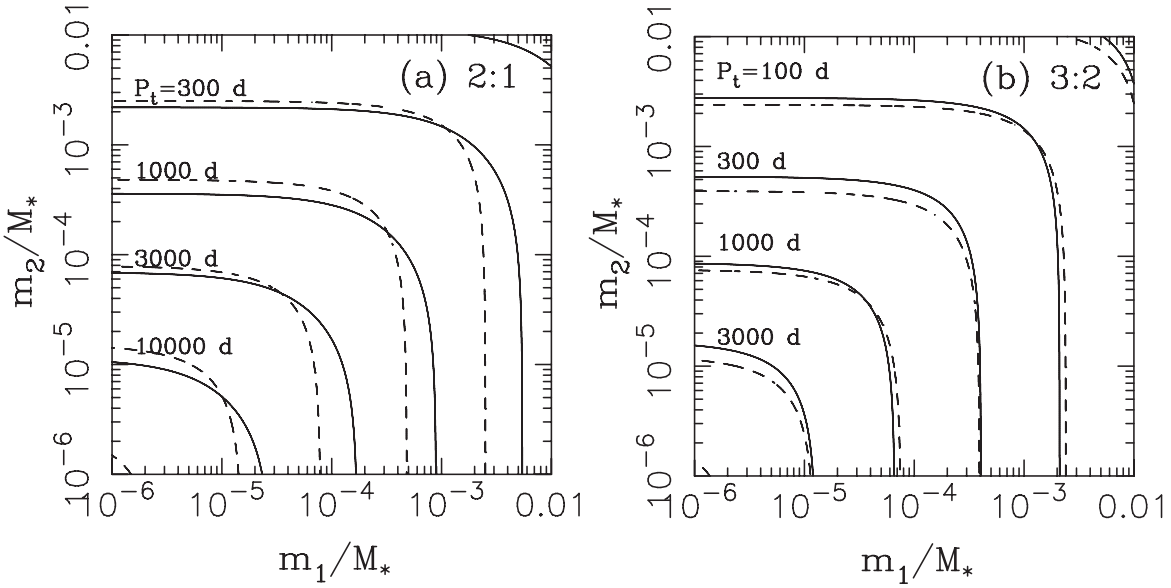

Figure 9. Libration period P_t as a function of scaled planetary masses m_1/M_* and m_2/M_* (solid lines). Here we assumed that $P_1 = 10$ days and $P_\tau = 3$ and computed $P_t = (\nu C^2)^{-1/3} P_\tau$. Panels (a) and (b) show the results for the 2:1 and 3:2 resonances, respectively. This is the expected TTV period produced by the resonant librations in these resonances. The dashed lines show the approximation from Equation (40), which becomes better for larger values of k (i.e., for $\alpha \to 1$).

Figure 9 shows the contour plots of P_t as a function of m_1/M_* and m_2/M_*. In the $\alpha \to 1$ limit, the period is proportional to $[(m_1 + m_2)/M_*]^{-2/3}$. A reasonable approximation of the period is then

$$P_t \simeq \frac{P_1 + P_2}{2} \frac{P_\tau}{2\pi} \left(\frac{m_1 + m_2}{M_*} \right)^{-2/3} \left[\frac{3}{2} k (k-1) |f_1| f_2 \right]^{-1/3}. \tag{40}$$

These considerations have important implications for the TTV period and its scaling with various parameters. For example, for two planets in the 2:1 resonance with $m_2/M_* = 10^{-4}$ and $m_1 \ll m_2$, the expected TTV period is $P_t \sim 78 P_1 P_\tau$. Thus, if $P_1 = 10$ days, and assuming that $P_\tau \sim 3$ in the libration regime, the TTV period will be $P_t \sim 6.4$ years. We can therefore very roughly write in this case

$$P_t(2{:}1) \sim 6.4 \text{ years} \times \frac{P_1}{10 \text{ days}} \frac{P_\tau}{3} \left(\frac{m_2/M_*}{10^{-4}} \right)^{-2/3}. \tag{41}$$

If, on the other hand, $m_1/M_* = 10^{-4}$ and $m_1 \gg m_2$, then the period will be approximately twice as long because of having P_2 in Equation (39) (instead of P_1 in Equation (38)). Finally, if $m_1/M_* = m_2/M_* = 10^{-4}$, then $P_t(2{:}\,1) \sim 4.5$ years. The periods in the $k > 2$ resonances are expected to be shorter (Figure 9(b)).

3.8. Approximation of Near-resonant Orbits

Lithwick et al. (2012; hereafter L12) derived elegant TTV expressions for two planets near (but not in) the first-order resonance. Here we discuss the relationship of these expressions to the results obtained here. Let us consider the Hamiltonian in Equations (14) and (16)

$$\mathcal{H} = n_s(\Gamma_1 + \Gamma_2) - \nu(\Gamma_1 + \Gamma_2)^2 + \beta_1 \sqrt{2\Gamma_1} \cos\sigma_1 + \beta_2 \sqrt{2\Gamma_2} \cos\sigma_2, \tag{42}$$

where we denote $\beta_1 = -Gm_1 m_2 A/a_2^*$ and $\beta_2 = -Gm_1 m_2 B/a_2^*$. We assume that the orbital eccentricities are small and that the two orbits are far enough from the resonance such that the term $\nu(\Gamma_1 + \Gamma_2)^2$ can be neglected. Introducing x_j and y_j from Equation (17) into Equation (42), we find that

$$\mathcal{H} = \frac{n_s}{2}[x_1^2 + y_1^2 + x_2^2 + y_2^2] + \beta_1 x_1 + \beta_2 x_2. \tag{43}$$

This Hamiltonian has a simple solution (e.g., Batygin & Morbidelli 2013b). Defining complex variables $z_j = x_j + \imath y_j$, the solution can be written as

$$z_j = -\frac{\beta_j}{n_s} + C_j \exp(\imath n_s t), \tag{44}$$

where C_j are integration constants related to the initial conditions. Now, since $\sigma_j = \theta - \varpi_j$, we can define L12's "complex eccentricities" $w_j = e_j \exp(\imath \varpi_j)$ and recast the approximate solution (44) as

$$w_j = \frac{\bar{C}_j}{\sqrt{\Lambda_1^*}} \exp \imath\theta_0 - \frac{\beta_j}{n_s \sqrt{\Lambda_1^*}} \exp \imath\theta, \tag{45}$$

where $\bar{C}_j$ is the complex conjugate of C_j. Here we assumed that $\theta = \theta_0 + n_s t$ and replaced $\Lambda_j \to \Lambda_j^*$. These assumptions are equivalent to those of L12, where the unperturbed (Keplerian) solution was inserted into the right-hand sides of the Lagrange equations, and the linearized solution was found by quadrature.

Equation (45) can be compared to Equation (A15) in L12. The first term in Equation (45) is constant and corresponds to the "free" term in Equation (A15). The second term in Equation (45) is identical to the second term in Equation (A15) (this can be trivially shown by resolving notation differences). L12 proceeded by using the constants K_1 and K_2 (Equation (13)) to derive expressions for $a_j(t)$, which were

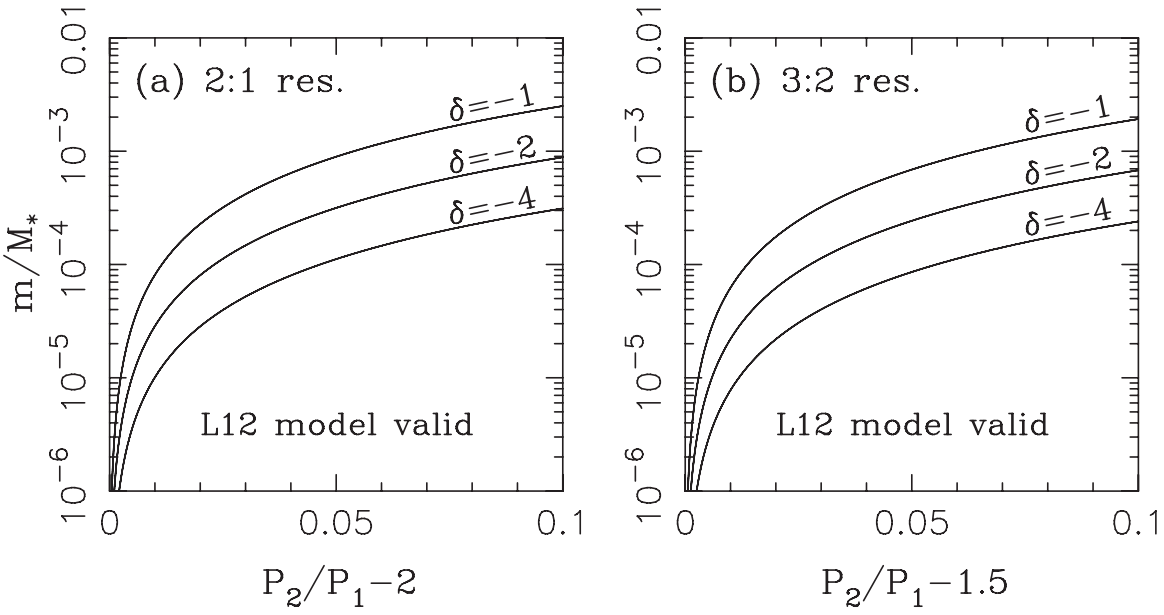

Figure 10. Validity domain of the L12 model. Here we assumed $m_1 \simeq m_2 = m$ and small orbital eccentricities and plotted the isolines of δ from Equation (23) as a function of planetary mass and $P_2/P_1 - k/(k-1)$. According to the discussion in the main text, the L12 model is valid for $\delta \lesssim -2$. This condition represents a combined constraint on the orbital period ratio and planetary masses. The parameter region below and to the right of the $\delta = -2$ line is where L12's TTV formula is strictly valid. This region covers most of the period range shown here for planetary masses below that of Saturn.

then used to obtain $\lambda_j = n_j t$ with $n_j = \sqrt{GM_*/a_j^3(t)}$.[7] Finally, L12 used a formula equivalent to Equation (1) to compute TTVs. None of these steps requires a special clarification.

The main assumption of L12 was therefore to (effectively) neglect the term $\nu(\Gamma_1 + \Gamma_2)^2$ in Equation (42). For this to be valid, $|n_s| \gg \nu(\Gamma_1 + \Gamma_2)$. Assuming that the masses and eccentricities of the two planets are comparable, and neglecting all factors of the order of unity, this condition can be written as $e_j^2 \ll |P_2/P_1 - k/(k-1)|$. This shows that the eccentricities cannot exceed a certain threshold for the L12 formulas to be valid. This threshold is not excessively restrictive. For example, for planetary orbits just outside the 2:1 resonance with $P_2/P_1 - 2 = 0.05$, the eccentricities need to be $e_j \ll \sqrt{0.05} = 0.22$.

In addition to the above eccentricity condition, the planetary orbits cannot be too close to a resonance where the nonlinear effects become important, even for negligible eccentricities. We tested this condition assuming initial orbits with small eccentricities and found that the L12 model is perfectly valid for $\delta < -4$. A small, ∼10% discrepancy in both the amplitude and frequency of w_j appears for $\delta \simeq -2$. A further increase of δ leads to a situation where Equation (45) is no longer an adequate representation of the resonant dynamics. According to our tests with $e_1 \simeq e_2 \lesssim 0.01$, the L12 model cannot usually be trusted for $\delta > -1$. Figure 10 shows these thresholds as a function of the planetary mass and orbit period ratio.

[7] The method of L12 ignores the contribution to λ_j from the derivatives of the Laplace coefficients. This is a correct assumption for the near-resonant orbits because these terms have n_s in the denominator, while the terms from $n_j(t)$ have n_s^2 in the denominator. The latter terms are thus amplified near a resonance where n_s is small.

4. TRANSIT TIMING VARIATIONS

If the variation of orbital elements is small, the TTVs of two planets, δt_1 and δt_2, can be computed from

$$-n_j \delta t_j = \delta\lambda_j + 2(\delta k_j \sin\lambda_j^* - \delta h_j \cos\lambda_j^*) + \mathcal{O}(e) \qquad (46)$$

(see, for example, Nesvorný & Morbidelli 2008). Here, $k_j = e_j \cos\varpi_j$, $h_j = e_j \sin\varpi_j$, and $\lambda_j = \lambda_j^* + \delta\lambda_j$, where $\lambda_j^* = n_j(t - t_0)$ with constant n_j. If the reference frame is chosen such that the orbital angles are measured with respect to the line of sight, transits occur when $\lambda_j^* \simeq 0$ (assuming small eccentricities). We therefore have $-n_j\delta t_j = \delta\lambda_j - 2\delta h_j + \mathcal{O}(e)$. The first-order eccentricity terms, which can be used to improve the validity for higher eccentricities, were given in Nesvorný (2009).

TTVs will thus have a contribution from the mean longitude variation, $\delta\lambda_j$, and another contribution from the variation of eccentricity and apsidal longitude, $\delta h_j = \delta(e_j \sin\varpi_j)$. Defining $Y_j = -\sqrt{2\Gamma_j}\sin\varpi_j$, we have for small eccentricities that $\Gamma_j \simeq \frac{1}{2}\Lambda_j e_j^2$ and $h_j = -Y_j/\sqrt{\Lambda_j}$. We then write $\Lambda_j = \Lambda_j^* + \delta\Lambda_j$ with constant Λ_j^* and obtain

$$-n_j\delta t_j = \delta\lambda_j + \frac{2}{\sqrt{\Lambda_j^*}}\delta Y_j + \mathcal{O}(e), \qquad (47)$$

where we retained only the first-order terms in small variations.

It remains to compute $\delta\lambda_j$ and δY_j. As for $\delta\lambda_j$, we have $d\lambda_j/dt = \partial\mathcal{H}_K/\partial K_j$, where $\mathcal{H}_K$ is given in Equation (14) (note that K_j appears in the n_s term in (15)). Substituting $\Gamma_1 + \Gamma_2 \to \Phi_1 + \Phi_2$ in Equation (14), taking the derivative with respect to K_j, and integrating with respect to t, we

obtain

$$\lambda_1 = \left[4 - \frac{3}{\Lambda_1^*}(K_1 - (k-1)\Phi_2)\right] n_1 (t - t_0) + 3(k-1)\frac{n_1}{\Lambda_1^*}\int_{t_0}^{t} \Phi_1 dt,$$
$$\lambda_2 = \left[4 - \frac{3}{\Lambda_2^*}(K_2 + k\Phi_2)\right] n_2 (t - t_0) - 3k\frac{n_2}{\Lambda_2^*}\int_{t_0}^{t} \Phi_1 dt. \quad (48)$$

Using the scaling relationship from Equations (24) and (27), we have that

$$\int_{t_0}^{t} \Phi_1(t) dt = \frac{1}{\nu}\int_{\tau_0}^{\tau} \Psi(\tau) d\tau, \quad (49)$$

where $\Psi(\tau)$ is given in Equation (31). The first terms in (48) describe a uniform circulation of angles λ_1 and λ_2 (note that $4n_j - 3K_j(n_j/\Lambda_j^*) = n_j$ for $e_j = 0$, as expected). They will not contribute to TTVs. Instead, TTVs will arise from the integral term. As the sign in front of the integral term is positive for λ_1 and negative for λ_2, the TTVs of the two planets are anticorrelated. The amplitudes of δt_1 and δt_2, denoted here by $A_{\lambda,1}$ and $A_{\lambda,2}$, satisfy

$$\frac{A_{\lambda,1}}{A_{\lambda,2}} = \frac{k-1}{k}\frac{\Lambda_2^*}{\Lambda_1^*} \simeq \left(\frac{k-1}{k}\right)^{2/3}\frac{m_2}{m_1}. \quad (50)$$

Thus, apart from a coefficient of the order of unity, the ratio of the TTV amplitudes from the λ terms is expected to be equal to the inverse of the planetary mass ratio.

As for δY_j, we have

$$Y_1 = \frac{1}{\sqrt{A^2 + B^2}}[A(v_1\cos\theta - u_1\sin\theta) + BV_2],$$
$$Y_2 = \frac{1}{\sqrt{A^2 + B^2}}[B(v_1\cos\theta - u_1\sin\theta) - AV_2], \quad (51)$$

where u_1 and v_1 were defined in Equation (18). They are related to the Φ_1 and ϕ_1 variables via Equation (19). Expressions (51) are derived in Appendix B. As we show in Appendix B, V_2 is a constant of motion, does not contribute to variations, and does not need to be computed.

Since the coefficients f_1 and f_2 have opposite signs (Table 1), A and B in Equation (51) will also have opposite signs, and the TTVs of the two planets will be anticorrelated. TTVs arising from the terms in (51) will have amplitudes $A_{h,1}$ and $A_{h,2}$ such that

$$\frac{A_{h,1}}{A_{h,2}} = \frac{n_2}{n_1}\frac{A}{B}\sqrt{\frac{\Lambda_2^*}{\Lambda_1^*}} \simeq \left(\frac{k-1}{k}\right)^{2/3}\frac{f_1}{f_2}\frac{m_2}{m_1}. \quad (52)$$

The ratio of TTV amplitudes from the h terms is inversely proportional to the ratio of planetary masses. This is the same mass dependence as in Equation (50). Thus, while the resonant TTV period discussed in Section 3.7 can be used to constrain m_1/M_* or m_2/M_*, the TTV amplitude ratio is sensitive to m_2/m_1.

Above we reduced the problem at hand to the evaluation of $v_1\cos\theta - u_1\sin\theta$. The θ terms are simple. From Equation (48) we have that

$$\theta = [n_s - 2\nu\Phi_2](t - t_0) - 2\nu\int_{t_0}^{t} \Phi_1 dt. \quad (53)$$

As for the u_1 and v_1 terms, we obtain

$$u_1 = \eta_1^{-1/3}\sqrt{2\Psi}\cos\psi = -\eta_1^{-1/3}[h_0 + (\Psi - \delta)^2],$$
$$v_1 = \eta_1^{-1/3}\sqrt{2\Psi}\sin\psi = -\eta_1^{-1/3}\frac{d\Psi}{d\tau}. \quad (54)$$

This is all we need for the computation of TTVs. To summarize, $\Psi(\tau)$ from Equation (31) needs to be inserted into (49) and (54). The integral in (49) needs to be computed and substituted into Equations (48) and (53). Then, θ, u_1, and v_1 obtained from Equations (53) and (54) are substituted into (51). The constant terms in λ_j and Y_j can be neglected because they do not contribute to TTVs. Finally, Equation (47) is used to compute the TTVs.

In principle, the method outlined above can be used to derive fully analytic expressions for δt_1 and δt_2, which would have the same general validity for low eccentricities as the analytic solution (31). For that, however, we would need to compute the derivative (needed for v_1) and integral (needed for λ_j and θ) of $\Psi(\tau)$ from (31). The integral ends up producing complex expressions (Appendix C). Here we therefore opt for a different approach, where we seek to find an expression for resonant TTVs in terms of the Fourier series.

4.1. Fourier Series Expansion

The solution (31) is valid for any initial condition (ψ_0, Ψ_0). Here we are not primarily interested in finding a general TTV expression for any (ψ_0, Ψ_0). Instead, our primary goal is to understand the general scaling of TTVs with planetary masses, resonant amplitude, and so on. We therefore opt for setting $\sin\psi_0 = 0$. This simplifies (31) considerably. Specifically, $\sin\psi_0 = 0$ implies that $f_0 = 0$, and (31) becomes

$$\Psi(\tau) = \Psi_0 + \frac{C_1}{4}\frac{1 - \mathrm{cn}(u,k)}{a + b\ \mathrm{cn}(u,k)}, \quad (55)$$

where we denoted $a = \gamma + e_2 - C_2/24$, $b = \gamma - e_2 + C_2/24$, and $\gamma = \sqrt{9\alpha^2 + \beta^2}$. This equation is valid in the domain $\Delta < 0$ shown in Figure 6, which includes the whole resonant libration zone. We used Equation (34) to relate the Weierstrass functions in (31) to the Jacobi functions. At the equilibrium point, $\Delta = 0$, $b = 0$, and $a = 2(\Psi_{eq} - \delta)^2 + \sqrt{2\Psi_{eq}}$ (Appendix A). For librations around the equilibrium point, we have that $a \gg b$ (Figure 11). We therefore identify a small parameter $\epsilon = b/a \ll 1$ and expand Equation (55) in the Taylor series in ϵ.

Retaining only the first-order terms in ϵ (approximation of low-amplitude librations), we obtain

$$\Psi(\tau) = \Psi_0 + \frac{C_1}{4a}[1 - (1+\epsilon)\mathrm{cn}(u,k) + \epsilon\ \mathrm{cn}^2(u,k)] + \mathcal{O}(\epsilon^2). \quad (56)$$

Including higher-order terms in ϵ would improve the validity of the approximation for large libration amplitudes. Next, we

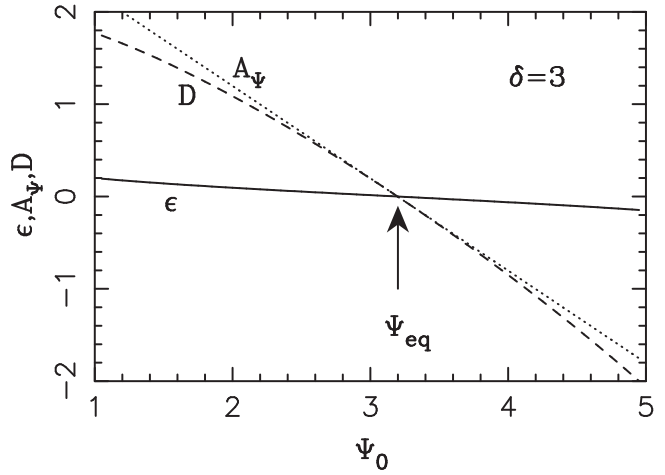

Figure 11. Dependence of various parameters of the analytic model on initial conditions. Here we set $\delta = 3$ and $\psi_0 = \pi$ and vary Ψ_0. The solid line shows the small parameter $\epsilon = b/a$. It is zero at the equilibrium point $\Psi_0 = \Psi_{\rm eq}$ (labeled by the arrow) and increases to $\epsilon \simeq 0.2$ near the separatrices. The dotted line shows the amplitude $A_\Psi = \Psi_0 - \Psi_{\rm eq}$. The parameter $D = C_1/4a$ (Section 4.1), shown by the dashed line, is an excellent approximation of A_Ψ for small-amplitude librations.

express cn and cn^2 in the Fourier series:

$$\mathrm{cn}(u,\,k) = \frac{2\pi}{k\mathbb{K}} \sum_{n=1}^{\infty} \frac{q^{n-1/2}}{1+q^{2n-1}} \cos\frac{(2n-1)\pi}{2\mathbb{K}} u \qquad (57)$$

and

$$\mathrm{cn}^2(u,\,k) = \frac{\mathbb{E}-k'^2\mathbb{K}}{k^2\mathbb{K}} + \frac{2\pi^2}{k^2\mathbb{K}^2} \sum_{n=1}^{\infty} \frac{nq^n}{1-q^{2n}} \cos\frac{n\pi}{\mathbb{K}} u. \qquad (58)$$

Here we have $k' = \sqrt{1-k^2}$ and $q = \exp(-\pi\mathbb{K}'/\mathbb{K})$ with $\mathbb{K}' = \mathbb{K}(k')$. Here, $\mathbb{E}(k)$ is the complete elliptic integral of the second kind. General expressions for $\mathrm{cn}^m(u,\,k)$, which can become useful when higher-order terms in (56) are accounted for, can be found in Kiper (1984).

Both of these Fourier series converge very rapidly, and we can therefore afford to use the lowest harmonics. In practice, given that the evaluation of u_1 from Equation (54) will require a multiplication of the Fourier series, here we consider only the first and second harmonics of $u = 2\sqrt{\gamma}(\tau - \tau_0)$. After substituting these terms into Equation (56), we obtain

$$\Psi = \Psi_0 + D\left(1+\frac{\epsilon}{2}\right) - D(1+\epsilon)\cos f_\tau \tau + \frac{1}{2} D\epsilon \cos 2f_\tau \tau. \qquad (59)$$

Here we denoted the frequency $f_\tau = 2\pi/P_\tau = \pi\sqrt{\gamma}/\mathbb{K}$ and $D = C_1/4a$. To simplify things, we set $\tau_0 = 0$ and drop all multiplication terms appearing from Equations (57) and (58) that are $\simeq 1$.[8]

Note that D is a proxy for the libration amplitude of Ψ (Figure 11). Equation (59) can be used to trivially compute the integral $\int \Psi d\tau$ appearing in Equation (49), which is then inserted into Equations (48) and (53). In the following text, the two TTV contributions, $\delta\lambda_j$ and δY_j, will be considered separately.

[8] Specifically, except for k very close to 1, we have $(\mathbb{E}-k'^2\mathbb{K})/(k^2\mathbb{K}) \simeq 1/2$, $2\pi\sqrt{q}/[k\mathbb{K}(1+q)] \simeq 1$, and $2\pi^2 q/[k^2\mathbb{K}^2(1-q^2)] \simeq 1/2$.

4.2. Contribution from Mean Longitude Variations

The calculation of $\delta\lambda_j$ is simple. Retaining the periodic terms in Equation (48), we obtain

$$\delta\lambda_1 = -3(k-1)\frac{n_1}{\Lambda_1^*\nu}\frac{P_\tau}{2\pi} D\,[C_{\lambda,1}\sin ft + C_{\lambda,2}\sin 2ft],$$
$$\delta\lambda_2 = 3k\frac{n_2}{\Lambda_2^*\nu}\frac{P_\tau}{2\pi} D\,[C_{\lambda,1}\sin ft + C_{\lambda,2}\sin 2ft]. \qquad (60)$$

with the coefficients $C_{\lambda,1} = 1+\epsilon$ and $C_{\lambda,2} = -\epsilon/4$ and frequency $f = \eta_2^{1/3} f_\tau = \eta_2^{1/3}\pi\sqrt{\gamma}/\mathbb{K}$ (Section 3.7).

These equations are the source of Equation (2) in Section 2, where we give the final expressions for TTVs arising from the variation of λ_1 and λ_2. In Equation (2), we have taken the liberty to drop the star from Λ_j^*, but it is understood that n_j, Λ_j, and other quantities depending on these parameters in Equation (2) are considered to be constant. Also, since D is a good proxy for the amplitude A_Ψ, we replaced $D \to A_\Psi$ in Equation (2). Note that A_Ψ is positive for $\Psi_0 > \Psi_{\rm eq}$ and negative for $\Psi_0 < \Psi_{\rm eq}$.

4.3. Contribution from Eccentricity and Apsidal Longitude

We need to compute $v_1\cos\theta - u_1\sin\theta$ and insert it in Equation (51). As for the terms including θ, we obtain from Equations (49), (53), and (59)

$$\theta = \theta_0 + f_\theta t + C_{\theta,1}\sin ft + C_{\theta,2}\sin 2ft, \qquad (61)$$

where

$$f_\theta = n_{\rm s} - 2\nu\Phi_2 - 2\eta_2^{1/3}\left[\Psi_0 + D\left(1+\frac{\epsilon}{2}\right)\right],$$
$$C_{\theta,1} = \frac{P_\tau}{2\pi} D(1+\epsilon),$$
$$C_{\theta,2} = -\frac{P_\tau}{2\pi} D\epsilon. \qquad (62)$$

We then use the following expansions to obtain $\cos\theta$ and $\sin\theta$:

$$\cos(x\sin\varphi) = J_0(x) + 2\sum_{n=1}^{\infty} J_{2n}(x)\cos 2n\varphi,$$
$$\sin(x\sin\varphi) = 2\sum_{n=1}^{\infty} J_{2n-1}(x)\sin(2n-1)\varphi, \qquad (63)$$

where $J_n(x)$ are the Bessel functions. Both these Fourier series converge rapidly for $x \ll 1$. We therefore retain only the lowest-order harmonics. This leads to

$$\begin{aligned}\cos\theta &= J_0(C_{\theta,1})\cos(\theta_0 + f_\theta t)\\ &\quad - 2J_1(C_{\theta,1})\sin(\theta_0 + f_\theta t)\sin ft\\ &\quad + 2J_2(C_{\theta,1})\cos(\theta_0 + f_\theta t)\cos 2ft,\\ \sin\theta &= J_0(C_{\theta,1})\sin(\theta_0 + f_\theta t)\\ &\quad + 2J_1(C_{\theta,1})\cos(\theta_0 + f_\theta t)\sin ft\\ &\quad + 2J_2(C_{\theta,1})\sin(\theta_0 + f_\theta t)\cos 2ft. \qquad (64)\end{aligned}$$

Here we neglected the coefficients $C_{\theta,2}$ that are of the order of ϵ (note that $\epsilon \ll D$; Figure 11).

The harmonics with f in Equation (64) appear from the resonant librations (Section 3.7). Since $\theta = \phi_1 - \zeta_1$ (Appendix B) and ϕ_1 oscillates around π in the libration island, θ has the same circulation frequency as ζ_1. Now, given

that ζ_1 is defined from the apsidal longitudes ϖ_1 and ϖ_2 (Appendix B), the interpretation of f_θ is that it is the mean precession frequency of the longitudes of periapsis. Neglecting terms $\mathcal{O}(\epsilon)$ and using the definition of δ in Equation (23), we find from (62) that

$$f_\theta = 2\eta_2^{1/3}(\delta - \Psi_{\rm eq}), \quad (65)$$

where $\Psi_0 + D \rightarrow \Psi_{\rm eq}$ is substituted (see Figure 11). The f_θ frequency therefore scales in the same manner with planetary parameters as $f = \eta_2^{1/3} f_\tau$ (as expressed by the $\eta_2^{1/3}$ factor). Unlike f, which derives from $f_\tau = 2\pi/P_\tau \sim 3$ in the libration island, f_θ contains the factor $2(\delta - \Psi_{\rm eq})$. This factor is $\ll 1$ (compare the dotted and solid "stable 1" lines in Figure 4). Therefore, f_θ is substantially smaller than f, which shows that the variations from θ are expected to occur on a long timescale.

Specifically, the period $P_\theta = 2\pi/f_\theta = \pi/(\delta - \Psi_{\rm eq})$ is equal to 10.1 for $\delta = 1$, 13.3 for $\delta = 2$, and 18.1 for $\delta = 4$. The longer periods for larger δ values are a consequence of $\Psi_{\rm eq}$ approaching δ for increasing values of δ (Section 3.5). Note that P_θ, at least in the approximation adopted here, is independent of the libration amplitude. Also, given that $\delta - \Psi_{\rm eq} < 0$ in the libration island, the f_θ frequency is negative as well, meaning that the circulation of θ is retrograde (implying retrograde rotation of ϖ_1 and ϖ_2).

The terms in Equation (64) containing frequencies f_θ and f could be combined to produce harmonics with frequencies $f_\theta \pm f$ and $f_\theta \pm 2f$. Given that, as we discussed above, the characteristic periods of these terms are largely different, we prefer to leave them multiplying each other in Equation (64). Accordingly, Equation (64) is interpreted as the resonant variations around the mean value that is slowly modulated with frequency f_θ.

The expressions for u_1 and v_1 are derived from Equation (54) after substituting Ψ from Equation (59). After some algebra we obtain

$$\begin{aligned} u_1 &= \eta_1^{-1/3} D (C_{u,0} + C_{u,1}\cos ft \\ &\quad + C_{u,2}\cos 2ft + C_{u,3}\cos 3ft), \\ v_1 &= \eta_1^{-1/3}\frac{2\pi}{P_\tau} D(-(1+\epsilon)\sin ft + \epsilon \sin 2ft) \end{aligned} \quad (66)$$

with coefficients

$$\begin{aligned} C_{u,0} &= \frac{u_0}{D} - D\left(\frac{3}{2} + 2\epsilon\right) - (2+\epsilon)(\Psi_0 - \delta), \\ C_{u,1} &= D\left(2 + \frac{7}{2}\epsilon\right) + 2(1+\epsilon)(\Psi_0 - \delta), \\ C_{u,2} &= -D\left(\frac{1}{2} + 2\epsilon\right) - \epsilon(\Psi_0 - \delta), \\ C_{u,3} &= \frac{1}{2}\epsilon D. \end{aligned} \quad (67)$$

In the above expression for the coefficient $C_{u,0}$, u_0 denotes the initial value:

$$u_0 = \sqrt{2\Psi_0} = -h_0 - (\Psi_0 - \delta)^2. \quad (68)$$

Figure 12 compares Equation (66) with the exact solution of Equations (25) and (26). It shows that the approximation (66) is excellent for small libration amplitudes but loses precision for large libration amplitudes. This happens mainly because the terms $\mathcal{O}(\epsilon^2)$ were neglected in Equation (56). In principle, it should be possible to include these and higher-order terms and improve the validity of the Fourier approximation by producing more general expressions. We leave this for future work.

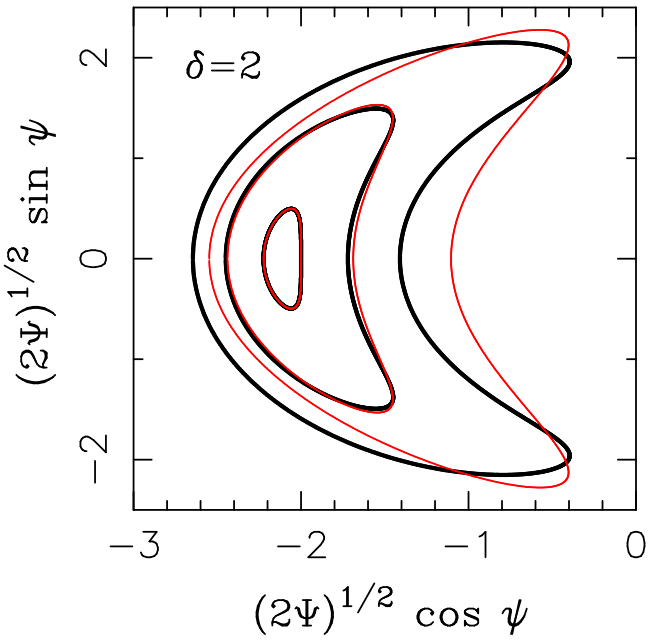

Figure 12. This plot illustrates the approximation (66). The bold black lines are the exact solution of the resonant Hamiltonian for $\delta = 2$ and three libration amplitudes. The red lines are the approximation given in Equation (66). The approximation is good for small libration amplitudes (inner curves) and degrades when the amplitude increases (outer curve).

Now we should combine Equations (64) and (66). Unfortunately, this generates a very long expression for δY_j. We do not explicitly give this equation here. The full expression was coded in a program and used to generate Figures 1 and 2. We find that the TTV terms from $v_1\cos\theta - u_1\sin\theta$ with the frequency f have amplitudes that are generally much smaller than the TTV amplitudes arising from the $\delta\lambda_j$ terms (Equation (60)). Here we therefore explicitly report only the most important harmonic with frequency f_θ. These terms do not have a counterpart in Equation (60). They are important for the long-term modulation of the TTV signal. Specifically, we find that

$$\begin{aligned} \delta Y_1 &= -\eta_1^{-1/3}\frac{AD}{\sqrt{A^2+B^2}} C_{u,0} J_0(C_{\theta,1})\sin(\theta_0 + f_\theta t), \\ \delta Y_2 &= -\eta_1^{-1/3}\frac{BD}{\sqrt{A^2+B^2}} C_{u,0} J_0(C_{\theta,1})\sin(\theta_0 + f_\theta t). \end{aligned} \quad (69)$$

This is the source of Equation (5). Since $J_0(C_{\theta,1}) \sim 1$, we do not list this term in Equation (5), where we also substitute $D \rightarrow A_\Psi$.

5. THE DOMAIN OF VALIDITY

We adopted several approximations in this work:

I. The Laplacian expansion of the perturbing function used in Section 3.1 is convergent only if the planetary eccentricities are small enough (Sundman 1912). For a planet on a circular orbit, this limits the validity of the expansion to $e < 0.25$ ($e < 0.2$) for orbits near its inner

(outer) 2:1 resonance, and to $e < 0.15$ ($e < 0.12$) for orbits near its inner (outer) 3:2 resonance. The analytic results derived here are not valid above these limits. See Nesvorný & Morbidelli (2008) for a discussion of Sundman's criterion.

II. All nonresonant terms were neglected in Section 3.1. The short-periodic terms with nonresonant frequencies produce short-periodic TTVs that can be calculated by the method described in Nesvorný & Morbidelli (2008). These terms can be linearly added to the expressions obtained here for resonant TTVs. The secular terms are second and higher orders in planetary eccentricities and contribute by only a small correction to the precession of orbits if the eccentricities are small.

III. The second- and higher-order resonant terms in planetary eccentricities were neglected in the perturbing function. This is an important approximation that limits the validity of the results to small eccentricities. The same assumption was adopted when writing δt_j as a variation of orbital elements.

IV. The amplitude of the semimajor axis variations was assumed to be small (this allowed us to simplify the Keplerian Hamiltonian in Section 3.3). The same assumption was adopted to compute δt_j from Equation (1), where we also neglected all second- and higher-order terms in small variations of the orbital elements. We find that these approximations are generally valid and do not impose any meaningful limits on the range of planetary parameters where our analytic results are valid.

V. The exact solution of the second fundamental model of resonance was expanded in the Taylor series in ϵ, and only the terms $\mathcal{O}(\epsilon)$ were retained (Section 4.1). In addition, the Jacobi elliptic functions were written as the Fourier series, and only the lowest harmonics were retained. Both these approximations limit the validity of our analytic TTV model to relatively small libration amplitudes. (In principle, the methods described in Section 4 can be used to obtain more general expressions.)

Here we perform tests of these assumptions to establish the domain of validity of our analytic model. To this end, we developed several codes that compute the resonant TTV signal at various stages of approximation. They are as follows:

A. A full N-body integrator of Equations (7) and (8), where the gravitational interaction of planets is taken into account exactly. We used the symplectic code known as `Swift` (Levison & Duncan 1994) with routines for an efficient and precise determination of TTVs (Nesvorný et al. 2013; see also Deck et al. 2014).

B. A numerical integrator in orbital elements that uses the Laplacian expansion of the perturbing function. Various terms can be included or excluded in this integrator. In the most basic approximation, the code includes only the first-order resonant terms from Equation (10). Optionally, it also accounts for the second-order secular or resonant terms. This code is used to test the approximations II and III listed above

C. A code that maps the initial orbital elements onto (22) and numerically integrates the corresponding Equations (25) and (26). Another code uses the exact analytic solution (31). As expected, these two codes give exactly the same result, which shows that our implementation of Equation (31) is working correctly.

D. A TTV code based on the analytic formulas derived in Section 4. This code is subject to all approximations discussed above. It cannot produce accurate results if the orbital eccentricities or libration amplitudes exceed certain limits.

We first test the approximation V. To this end we compare the results obtained with code B with the analytic results from method D. In B, we include the two first-order resonant terms and neglect terms that are second or higher order in planetary eccentricities.[9] The masses and initial orbits are chosen such that $\delta = 2$ (Figure 13) or $\delta = 4$ (Figure 14). The initial orbits are then varied to survey different libration amplitudes. These tests show that the analytic method produces very reliable results for $A_\Psi \lesssim 1$ (top panels in Figures 13 and 14). For the libration amplitudes much larger than that, our analytic expressions for u_1 and v_1 in Equation (66) become inaccurate (see Figure 12). As a consequence, the analytic approximation of the TTV terms from δh_j fails (bottom panels in Figures 13 and 14).

Interestingly, however, the analytic approximation of the *full* TTV signal is reasonable even if $A_\Psi > 1$. This happens because the TTV terms from $\delta\lambda_j$ increase with A_Ψ and become dominant for large A_Ψ. We are able to reproduce these terms correctly because the analytic formula in Equation (2) has a more general validity than the one that requires a correct approximation of the boomerang-shaped trajectories in the (u_1, v_1) plane (Equation (66)). We therefore conclude that the analytic TTV model can be used, with some caution, even if the libration amplitudes are relatively large.

We now turn our attention to the approximations I, II, and III. We find that the omission of the higher-order resonant terms in III is the most restrictive assumption. To illustrate this, Figures 15 (inner planet) and 16 (outer planet) show a comparison of the analytic model with TTVs computed from the N-body code (method A above). Here we set different planetary eccentricities ranging from $e_1 = e_2 = 0.001$ (left panels in both figures) to $e_1 = e_2 = 0.05$ (right panels). We find that the analytic model works well for $e_1 = e_2 = 0.001$.

Already for $e_1 = e_2 = 0.01$, a significant discrepancy appears (see middle panels in Figures 15 and 16). An important part of the discrepancy, however, is not due to assumption III, but is rather related to the choice of initial conditions. Recall that, in addition to the resonant terms, the exact computation of TTVs with method A also contains the short-periodic harmonics, while the analytic method D does not account for these terms. This presents a difficulty when choosing the initial conditions in A and D that are consistent with each other. If the same values are adopted in A and D, the initial semimajor axes in A generate slightly different values of the mean orbital frequencies than the same initial semimajor axes in D. This effect then propagates into a difference in the libration frequency f. To demostrate this, we surveyed a small neighborhood of the initial conditions and found that it is always possible, if the eccentricities are sufficiently small, to apply a small adjustment such that the difference between the analytical and numerical results vanishes (left and middle bottom panels in Figures 15 and 16). Note that this initial value

[9] The same comparison method was used to produce Figures 1 and 2 in Section 2.

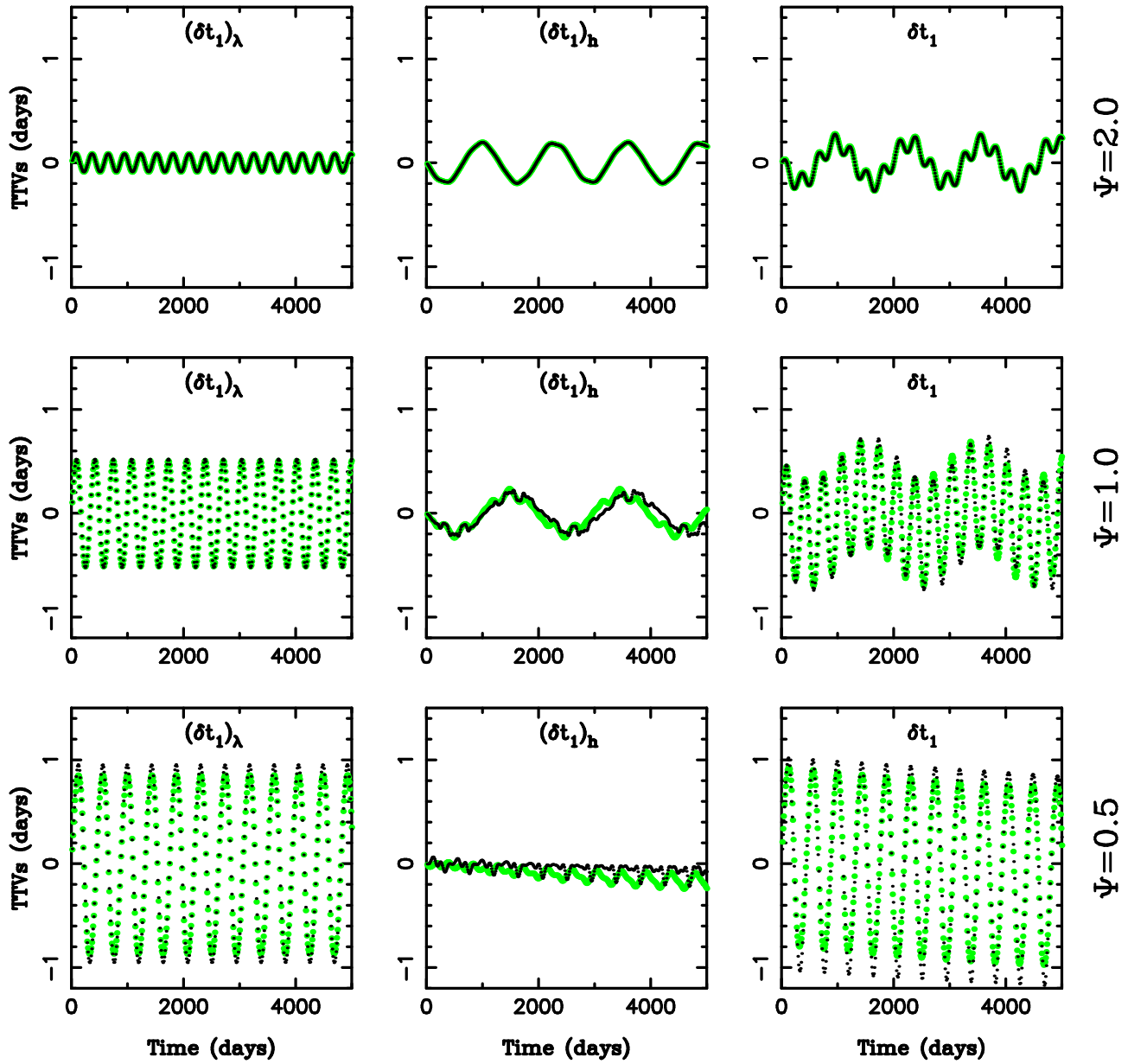

Figure 13. Tests of the validity of the analytic model for different libration amplitudes. The planetary masses and orbital parameters were chosen such that $\delta = 2$ in all cases shown here. We fixed $m_1 = m_2 = 3 \times 10^{-4}\, M_*$, $M_* = 1\, M_{\rm Sun}$, and $a_1 = 0.1$ au and varied a_2 near the external 3:2 resonance with the inner planet ($a_2 \simeq 0.131$ au). The eccentricities were adjusted to give $\delta = 2$ and a desired initial value Ψ_0. From top to bottom, the panels show the results for $\Psi_0 = 2$, $\Psi_0 = 2.5$, and $\Psi_0 = 3.5$. The stable equilibrium point is located at $\Psi_{\rm eq} = 2.24$ for $\delta = 2$. The different cases shown here thus correspond to the libration amplitudes $A_\Psi = 0.25$, 1.24, and 1.74 (from top to bottom). The plots show the TTVs of the inner planet (the results for the outer planet are similar). The green dots were obtained by numerically integrating the differential equations corresponding to the resonant Hamiltonian (9) and (10). The black lines were obtained from the analytic TTV expressions (1) and (2) and a generalization of (5) derived in Section 4.3. From left to right, the different panels show the TTVs from $\delta\lambda_j$ and δh_j and their sum from Equation (1).

problem does not seriously limit the application of the analytic model to the real data because it requires only a very small adjustment of a_1 or a_2 (or equivalently n_1 and n_2), which can easily be absorbed by other parameters.

Another more fundamental discrepancy appears for $e_1 = e_2 = 0.05$. In this case, the TTV frequency computed from the analytic model is nearly 40% higher than the actual frequency, and the TTV amplitudes are $\simeq$25% smaller than their actual values (right panels in Figures 15 and 16). In this case, it is not possible to adjust the initial conditions to cancel the difference. This shows that the assumption III starts to fail. We confirm this by method B, where it becomes apparent that including the second-order resonant terms improves the model's precision. Still, for $e_1 = e_2 = 0.05$, the amplitude discrepancy is relatively minor and can be compensated for, for example, by a relatively small correction of planetary masses. We therefore find that the analytic model is still useful in this case. Our additional tests show that the analytic expressions for TTVs are not reliable for eccentricities exceeding ~0.1. (The validity domain in e should be slightly larger for distant resonances such as 2:1 and smaller for $k \geqslant 4$.)

The analytic model was developed under the assumption of exactly coplanar planetary orbits. This assumption was used in Section 3.1 to neglect all terms in the Laplacian expansion of the perturbing function that depend on inclinations. The model is therefore not expected to be valid if the mutual inclination

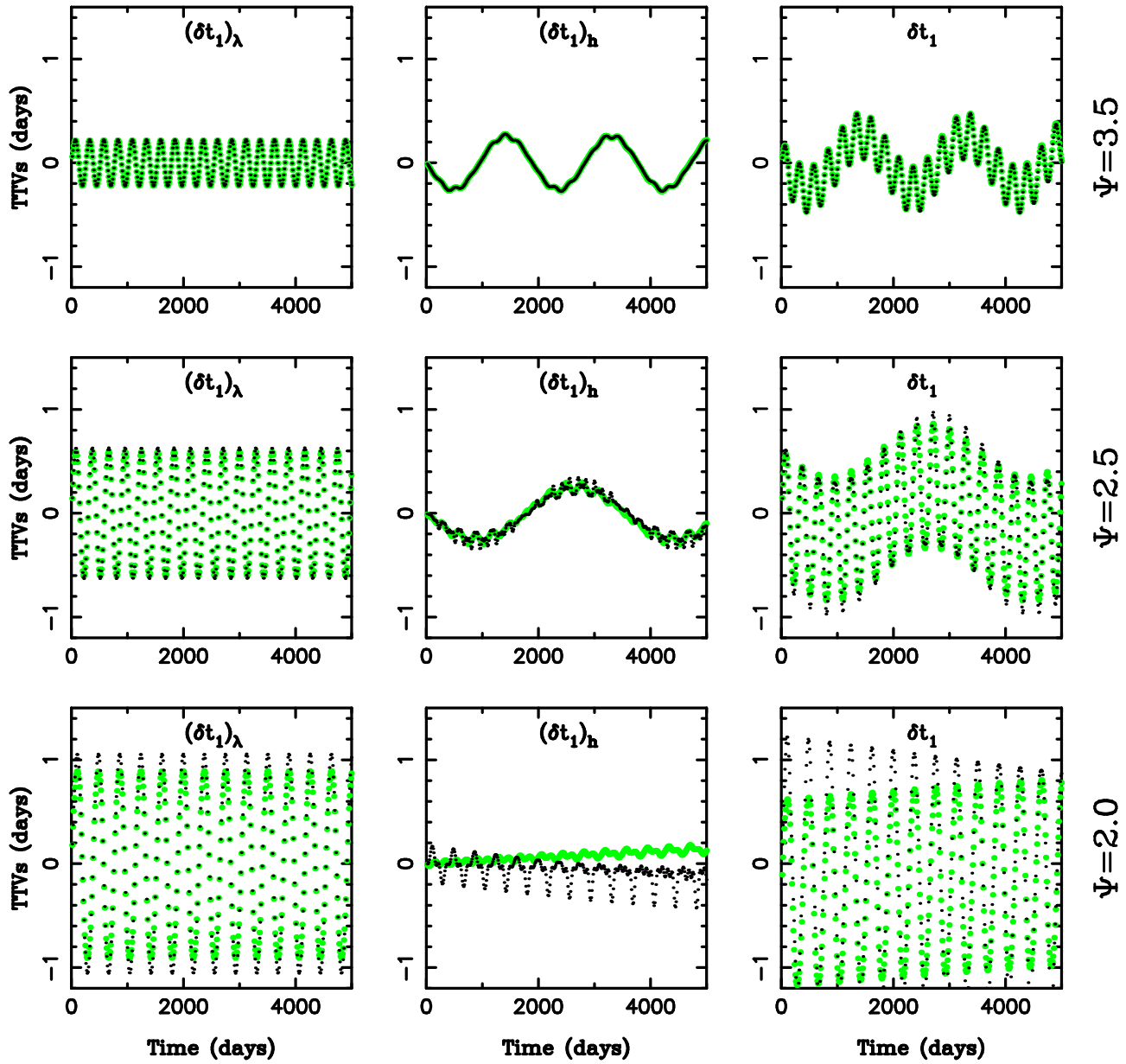

Figure 14. Same as Figure 13 but for $\delta = 4$. In this case, the stable equilibrium point is at $\Psi_{\rm eq} = 4.14$. From top to bottom, the different panels correspond to $\Psi_0 = 3.5$ ($A_\Psi = 0.67$), $\Psi_0 = 2.5$ ($A_\Psi = 1.17$), and $\Psi_0 = 2$ ($A_\Psi = 1.57$).

between orbits, $I_{\rm mutual}$, is large. We performed various tests of this assumption and found that the analytic model is reasonably accurate for $I_{\rm mutual} < 10^\circ$ but fails to produce reliable results for $I_{\rm mutual} \gtrsim 10^\circ$. This should not be a severe limitation of the applicability of the analytic results to the multitransiting planetary systems because the orbits in these systems are expected to be nearly coplanar (e.g., Fang & Margot 2012).

6. CONCLUSIONS

In this work we developed an analytic model for TTVs of a pair of resonant planets and discussed how the TTV period and amplitude constrain the masses and orbits of the two planets. The model is strictly valid only for small orbital eccentricities ($e < 0.1$). It was developed under the assumption of coplanar orbits, but our tests show that it is valid even if the mutual inclination of orbits is not large ($<10^\circ$).

The resonant TTV signal is expected to contain the harmonics of two basic periods: the period of resonant librations and the period of apsidal precession of orbits. The latter is expected to be ~5 times longer than the former and may be difficult to detect with a short baseline of the TTV measurements. The libration period is relatively insensitive to the exact location of the system parameters in the resonant island and scales with $(m/M_*)^{-2/3}$. Its determination from the TTV measurements can therefore help to constrain the planetary masses. This is an important difference with respect to the near-resonant case (Lithwick et al. 2012), where the TTV period is the superperiod, which is independent of mass.

The TTV amplitudes, on the other hand, can be used to constrain the ratio of planetary masses m_1/m_2. Since both the TTV period and amplitude depend on the resonant amplitude A_Ψ, some mild degeneracies between the mass and orbital

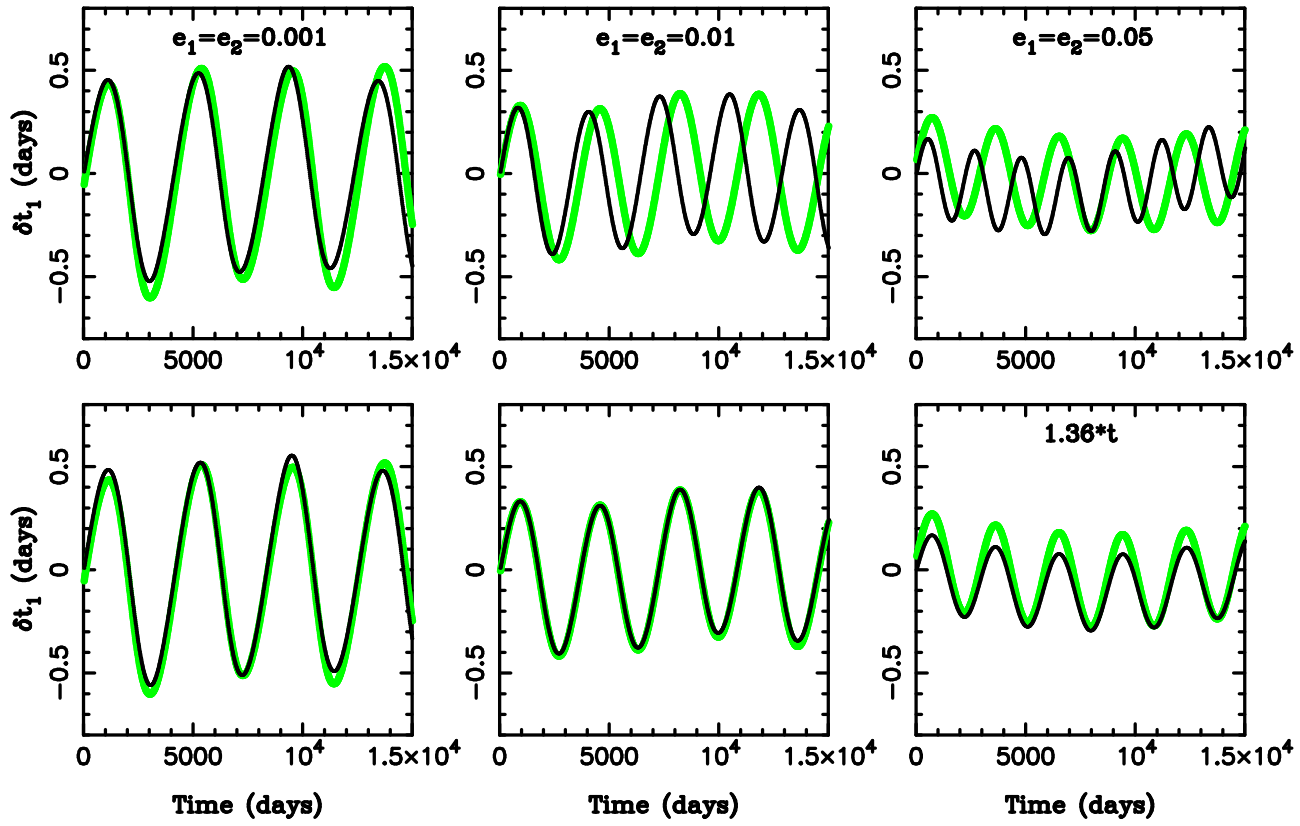

Figure 15. Comparison of TTVs obtained with the analytic model (black lines) and the precise N-body integrator (green lines). From left to right, the orbital eccentricities of planets were increased to test the validity of the analytic model. We fixed $m_1 = m_2 = 10^{-5}\,M_*$, $M_* = 1\,M_{\rm Sun}$, $a_1 = 0.1$ au, and a_2 near the external 3:2 resonance with the inner planet ($a_2 = 0.13095$ au). The TTVs of the inner planet are shown here. The case with $e_1 = e_2 = 0.001$ (left panels) corresponds to $\delta = 0.51$ and $\Psi_0 = 0.007$. The case with $e_1 = e_2 = 0.01$ (middle panels) corresponds to $\delta = 1.25$ and $\Psi_0 = 0.75$. The case with $e_1 = e_2 = 0.05$ corresponds to $\delta = 19.3$ and $\Psi_0 = 18.8$. In the two bottom panels on the left, we illustrate how a small adjustment of the initial conditions improves the results (see the main text for a discussion). In the bottom-right panel, we rescaled time to show that a modest adjustment of the frequency can resolve the discrepancy when eccentricities are larger.

parameters are expected, but these degeneracies can be broken by a detection of higher-order resonant harmonics, which constrain A_Ψ, or short-periodic (chopping) effects. A detailed analysis of this problem and the application of our analytic model to the resonant exoplanets (Winn & Fabrycky 2015) is left for future work.

The work of D.N. was supported by NASA's ADAP program. D.V. was supported by the Czech Grant Agency (grant P209-13-01308S). Slawek Breiter pointed out to us the general solution Equation (31) in Whittaker & Watson (1920). We thank Katherine Deck, Eric Agol, and an anonymous reviewer for useful comments on the manuscript.

APPENDIX A
PARAMETER $\epsilon = b/a$

The coefficients C_n in Equation (31) are obtained from the derivatives of $f(\Psi)$ with $\Psi = \Psi_0$:

$$C_1 = 2[1 - 2(\Psi_0 - \delta)\sqrt{2\Psi_0}],$$
$$C_2 = -4[2(\Psi_0 - \delta)^2 + \sqrt{2\Psi_0}]. \quad (70)$$

The expressions for C_3 and C_4 are not needed if we set $\psi_0 = \pi$ and thus $f_0 = 0$. The invariants in Equation (32) can be written as

$$g_2 = \frac{4}{3}\left(h_0^2 - \frac{3}{2}\delta\right),$$
$$g_3 = \frac{1}{4} - \frac{8}{27}h_0\left(h_0^2 - \frac{9}{4}\delta\right), \quad (71)$$

where we denoted $h_0 = -(\Psi_0 - \delta)^2 + \sqrt{2\Psi_0}$. The determinant Δ becomes

$$\Delta = -\frac{27}{16} - 8\delta^3 + 4h_0\left(h_0^2 + \delta^2 h_0 - \frac{9}{4}\delta\right). \quad (72)$$

If we define

$$F = \frac{1}{2}\left(g_3 + \frac{1}{3}\sqrt{-\frac{\Delta}{3}}\right)^{1/3}, \quad (73)$$

then the three roots of the cubic equation can be obtained from

$$\alpha = -\frac{1}{2}\left(F + \frac{g_2}{12F}\right),$$
$$\beta = \frac{1}{2\sqrt{3}}\left(F - \frac{g_2}{12F}\right),$$
$$e_2 = F + \frac{g_2}{12F} = -2\alpha. \quad (74)$$

In the equilibrium point, $\Psi_0 = \Psi_{\rm eq}$, we have that $\Delta = 0$, and thus $F = g_3^{1/3}/2$. It follows that $\beta = 0$ and

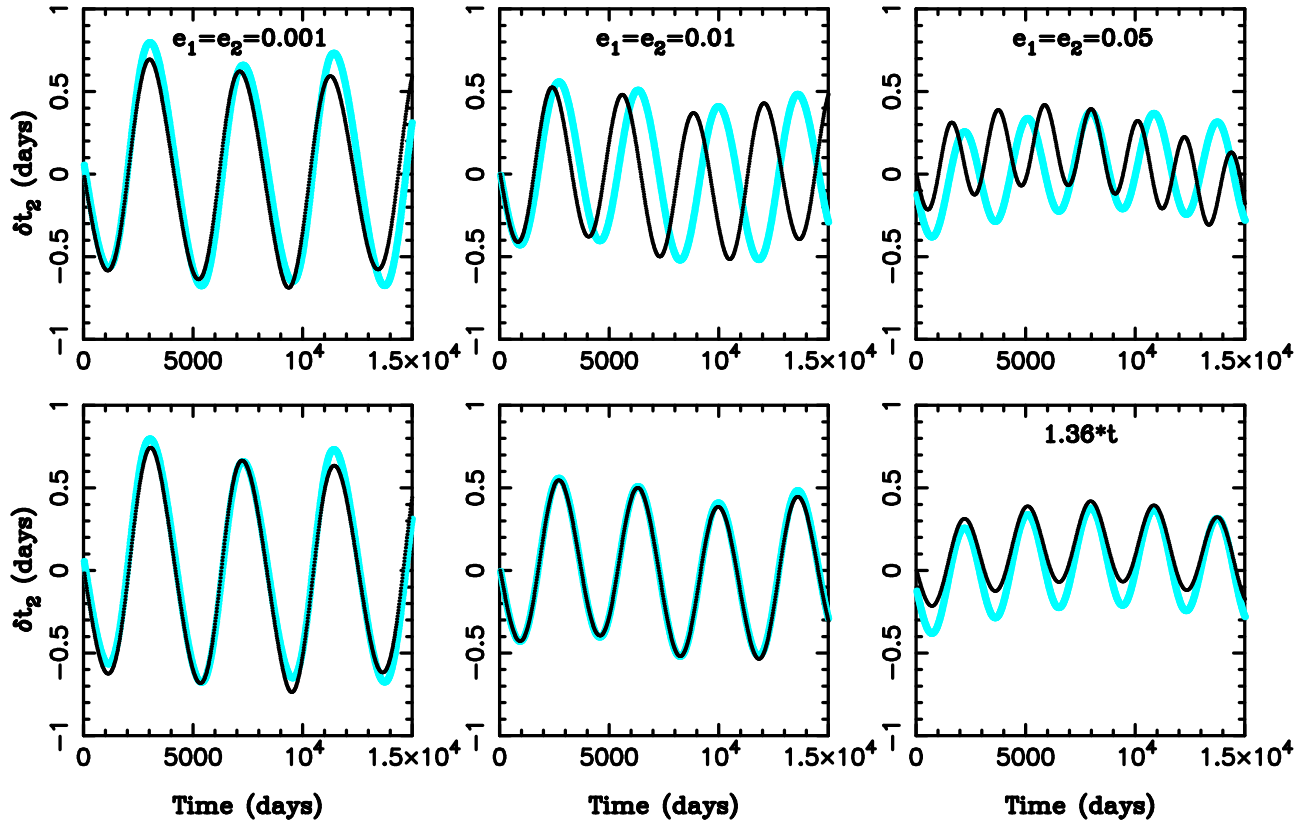

Figure 16. Same as Figure 15 but for TTVs of the outer planet.

$\alpha = -F = -g_3^{1/3}/2 = C_2/24 < 0$. Therefore, $b = 0$ and $a = -C_2/4$, where a and b are defined in the main text. Figure 11 shows $\epsilon = b/a$ for $\delta = 3$. It is zero at the equilibrium point and increases to $\epsilon \simeq 0.2$ at the separatrix. Higher values of δ lead to smaller values of ϵ. For $\delta \simeq 1$, on the other hand, ϵ can be as large as 0.6 near the separatrix.

APPENDIX B
EXPRESSIONS FOR Y_j

In Section 3 we omitted explaining one important issue that becomes apparent if the degree of freedom related to $\theta = k\lambda_2 - (k-1)\lambda_1$ is treated separately from those related to ϖ_1 and ϖ_2 (as was done in BM13). To explain this issue, we first define in direct correspondence to Equation (17)

$$X_1 = \sqrt{2\Gamma_1}\cos\gamma_1, \quad Y_1 = \sqrt{2\Gamma_1}\sin\gamma_1,$$
$$X_2 = \sqrt{2\Gamma_2}\cos\gamma_2, \quad Y_2 = \sqrt{2\Gamma_2}\sin\gamma_2, \tag{75}$$

where $\gamma_j = -\varpi_j$. Second, we perform a transformation (see Section 3.4) to the new variables (V_1, V_2; U_1, U_2):

$$U_1 = \frac{AX_1 + BX_2}{\sqrt{A^2+B^2}}, \quad V_1 = \frac{AY_1 + BY_2}{\sqrt{A^2+B^2}},$$
$$U_2 = \frac{BX_1 - AX_2}{\sqrt{A^2+B^2}}, \quad V_2 = \frac{BY_1 - AY_2}{\sqrt{A^2+B^2}}. \tag{76}$$

And last, we introduce new polar variables (ζ_1, ζ_2; Φ_1, Φ_2) such that

$$U_1 = \sqrt{2\Phi_1}\cos\zeta_1, \quad V_1 = \sqrt{2\Phi_1}\sin\zeta_1,$$
$$U_2 = \sqrt{2\Phi_2}\cos\zeta_2, \quad V_2 = \sqrt{2\Phi_2}\sin\zeta_2. \tag{77}$$

The inverse transformation to (76) is

$$X_1 = \frac{AU_1 + BU_2}{\sqrt{A^2+B^2}}, \quad Y_1 = \frac{AV_1 + BV_2}{\sqrt{A^2+B^2}},$$
$$X_2 = \frac{BU_1 - AU_2}{\sqrt{A^2+B^2}}, \quad Y_2 = \frac{BV_1 - AV_2}{\sqrt{A^2+B^2}}. \tag{78}$$

With these definitions, it is straightforward to show that $\phi_j = \theta + \zeta_j$, where ϕ_j are the original angles defined in (19), $\zeta_1 = \arg(AZ_1 + BZ_2)$, and $\zeta_2 = \arg(BZ_1 - AZ_2)$, where $Z_j = X_j + \imath Y_j = \sqrt{2\Gamma_j}\exp\imath\gamma_j$. We thus find that $V_1 = v_1\cos\theta - u_1\sin\theta$. When substituted into (78), we obtain Equation (51) in the main text. In addition, it can be shown that $d\zeta_2/dt = d\phi_2/dt - d\theta/dt = 0$. The angle ζ_2 is therefore constant. Consequently, since $\Phi_2 = $ const. as well, both U_2 and V_2 are constants of motion. This result is used in Section 4, where V_2 in Equation (51) does not contribute to TTVs.

APPENDIX C
INTEGRAL $\int \Psi d\tau$

The integral in Equation (49) with $\Psi(\tau)$ from Equation (55) admits the following exact solution:

$$\int \Psi(\tau)d\tau = \left(\Psi_0 - \frac{C_1}{4a\epsilon}\right)\tau + \frac{C_1(1+\epsilon)}{8a\epsilon\sqrt{\gamma}}\int \frac{du}{1+\epsilon\,\mathrm{cn}(u,k)}, \tag{79}$$

where $\epsilon = b/a$ and γ are defined in Section 4.1. From Byrd & Friedman (1971) (BF 341.03) we have

$$\int \frac{du}{1 + \epsilon\ \mathrm{cn}(u, k)} = \frac{1}{1 - \epsilon^2}[\Pi(\varphi, n, k) - \epsilon\ C\ \mathrm{atan}\left(\frac{\mathrm{sd}(u, k)}{C}\right)], \quad (80)$$

where $\Pi(\varphi, n, k)$ is the Legendre elliptic integral of the third kind, $\varphi = \mathrm{am}\, u$ is the Jacobi amplitude, and $\mathrm{sd}(u, k) = \mathrm{sn}(u, k)/\mathrm{dn}(u, k)$. The constants n and C are

$$n = \frac{\epsilon^2}{\epsilon^2 - 1}, \quad (81)$$

$$C = \sqrt{\frac{1 - \epsilon^2}{k^2 + \epsilon^2\ k'^2}}. \quad (82)$$

Note that Byrd & Friedman (1971) use a different notation for the coefficient n than Press et al. (2007). To use the numerical subroutines from Press et al. (2007), $n = \epsilon^2/(1 - \epsilon^2)$.

REFERENCES

Agol, E., & Deck, K. 2016, ApJ, 818, 177
Agol, E., Steffen, J., Sari, R., & Clarkson, W. 2005, MNRAS, 359, 567
Batygin, K., & Morbidelli, A. 2013a, A&A, 556, A28 (BM13)
Batygin, K., & Morbidelli, A. 2013b, AJ, 145, 1
Brouwer, D., & Clemence, G. M. 1961, Methods of Celestial Mechanics (New York: Academic)
Byrd, P. F., & Friedman, M. D. 1971, Handbook of Elliptic Integrals for Engineers and Scientists (Berlin: Springer)
Deck, K. M., & Agol, E. 2015, ApJ, 802, 116
Deck, K. M., & Agol, E. 2016, ApJ, 821, 96
Deck, K. M., Agol, E., Holman, M. J., & Nesvorný, D. 2014, ApJ, 787, 132
Fang, J., & Margot, J.-L. 2012, ApJ, 761, 92
Ferraz-Mello, S. 2007, Canonical Perturbation Theories (Berlin: Springer)
Hadden, S., & Lithwick, Y. 2016, ApJ, submitted (arXiv:1510.02476)
Henrard, J., & Lemaître, A. 1983, CeMDA, 30, 197
Henrard, J., Lemaître, A., Milani, A., & Murray, C. D. 1986, CeMDA, 38, 335
Heyl, J. S., & Gladman, B. J. 2007, MNRAS, 377, 1511
Holman, M. J., Fabrycky, D. C., Ragozzine, D., et al. 2010, Sci, 330, 51
Holman, M. J., & Murray, N. W. 2005, Sci, 307, 1288
Kiper, A. 1984, MaCom, 43, 247
Levison, H. F., & Duncan, M. J. 1994, Icar, 108, 18
Lissauer, J. J., Fabrycky, D. C., Ford, E. B., et al. 2011, Natur, 470, 53
Lithwick, Y., Xie, J., & Wu, Y. 2012, ApJ, 761, 122 (L12)
Masset, F., & Snellgrove, M. 2001, MNRAS, 320, L55
Miralda-Escudé, J. 2002, ApJ, 564, 1019
Nesvorný, D. 2009, ApJ, 701, 1116
Nesvorný, D., Kipping, D., Terrell, D., et al. 2013, ApJ, 777, 3
Nesvorný, D., Kipping, D. M., Buchhave, L. A., et al. 2012, Sci, 336, 1133
Nesvorný, D., & Morbidelli, A. 2008, ApJ, 688, 636
Nesvorný, D., & Vokrouhlický, D. 2014, ApJ, 790, 58
Press, W. H., Teukolsky, S. A., Vetterling, W. T., & Flannery, B. P. 2007, Numerical Recipes: The Art of Scientific Computing (Cambridge: Cambridge Univ. Press)
Sessin, W., & Ferraz-Mello, S. 1984, CeMec, 32, 307
Shinkin, V. N. 1995, CeMDA, 62, 323
Sundman, K. F. 1916, Ofversigt Finska Vetenskaps-Soc. Forth., 58A, 24
Vokrouhlický, D., & Nesvorný, D. 2014, ApJ, 791, 6
Whittaker, E. T., & Watson, G. N. 1920, A Course of Modern Analysis (Cambridge: Cambridge Univ. Press)
Winn, J. N., & Fabrycky, D. C. 2015, ARA&A, 53, 409
Wisdom, J. 1986, CeMDA, 38, 175